Chapter 03

Isolation of Oleanolic acid and development of its EGFR targeted albumin nanoparticles, and their cytotoxicity and pharmacokinetics evaluation for lung cancer therapy

3 Chapter 03: Isolation of Oleanolic acid and development of its EGFR targeted albumin nanoparticles, and their cytotoxicity and pharmacokinetics evaluation for lung cancer therapy

3.1 Objective

The objective of this study was to isolate oleanolic acid and to prepare EGFR targeted OLA loaded albumin nanoparticles (ALB-NPs) conjugated with cetuximab antibody for targeting EGFR receptors and to characterize prepared nanoformulations on the basis of their physicochemical properties such as shape, particle size, zeta-potential, surface morphology and surface chemistry, and developed ALB-NPs were evaluated for *in vitro* cytotoxicity against A549 cells and safety assessment via HEK-293 cells, *in vivo* pharmacokinetic, histopathology and *in vivo* anticancer efficacy in B(a)P induced lung cancer mice were performed.

3.2 Plan of Study

1. Isolation and purification of oleanolic acid.

2. Preparation and characterization of TPGS-SA.

3. Preparation and characterization of OLA-loaded albumin nanoparticles (OLA-ALB-NPs) using emulsification -solvent evaporation method.

4. Preparation of CTX conjugated EGFR targeted CTX-OLA-ALB-NPs using acid-amine coupling reaction.

5. Physicochemical and *in vitro* evaluation of EGFR-targeted CTX-OLA-ALB-NPs and OLA-ALB-NPs.

- ✓ Particle size, polydispersity index, and zeta potential.
- ✓ Electron microscopy (TEM & AFM).
- ✓ Crystallographic studies by XRD.
- ✓ Surface chemistry by XPS.

- ✓ Determination of entrapment efficiency.
- ✓ *In vitro* drug release studies.
- ✓ *In vitro* cellular uptake study on A549 cells.
- ✓ *In vitro* cytotoxicity on A549 and HEK-293 cells.

6. *In vivo* evaluation of EGFR-targeted ALB-NPs.

- ✓ Pharmacokinetic studies in Wistar rats.
- ✓ Histopathology studies in Wistar rats.
- ✓ Anticancer efficacy studies on B(a)P-induced lung cancer mice model.

3.3 Materials

Coumarin 6 (C6), Vitamin E polyethylene glycol succinate (Vitamin E-TPGS), N-(3-Dimethylaminopropyl)-N′-ethylcarbodiimide hydrochloride (EDC hydrochloride), N-hydroxysuccinimide (NHS), Pur-A-Lyzer™ midi dialysis kit (MWCO 1 kDa, capacity 50-800 µL) were purchased from Sigma Aldrich Chemicals Private Limited, Bengaluru, India. HiMedia Laboratories Pvt. Ltd., Mumbai, India, provided the foetal bovine serum (FBS) and bovine serum albumin (ALB). Merck Specialities Ltd. Mumbai, India, supplied cetuximab (Erbitux R). The National Centre for Cell Science (NCCS) national repository division in Pune, India, supplied the human lung cancer (A549) and HEK-293 cell lines. Thermo Fisher Scientific, Mumbai, India, provided trypsin-EDTA, 3-(4,5-dimethyl thiazolyl-2-yl)-2,5-diphenyltetrazolium bromide (MTT), Dulbecco's modified Eagle's medium (DMEM), and dead cell apoptosis kits with Annexin V for flow cytometry. Tarsons Products Limited, Kolkata, India, provided 96-well culture plates and culture flasks of various capacities. Merck provided HPLC-grade acetonitrile and methanol (Darmstadt, Germany). Millipore's Milli-Q filtration system was used to prepare deionized water (Molsheim, France). The rest of the chemicals were of analytical grade. All reagents, chemicals, and other consumables employed in other investigations were of molecular biology or analytical quality.

3.4 Methods

3.4.1 Extraction and isolation of oleanolic acid

The process of extracting OLA from *Lantana camara* dry roots was performed with some modifications (79). Initially, fresh Lantana camara roots were meticulously gathered and subjected to thorough cleaning to eliminate soil and organic residues. Subsequently, the cleaned roots were cut into small fragments and air-dried in a shaded location. After complete drying, the roots were pulverized into a fine powder using a grinder. The resulting 800 g of powdered *Lantana camara* roots underwent a cold defatting procedure with hexane, followed by four successive overnight extractions with methanol (MeOH) at room temperature. The extraction process continued for 8 hours until the material was completely exhausted. Afterward, the solvent was evaporated under a vacuum at 40 ºC, forming a brownish viscous substance, constituting the crude extract. To enhance the purity of the crude extract, it was dissolved in an excess of ethyl acetate (EtoAC) and left to stand at room temperature overnight. The resultant mixture underwent filtration and subsequent concentration under reduced pressure at 45 ºC. The concentrated extract obtained was further processed using silica gel column chromatography. This involved employing a range of hexane-ethyl acetate elution solvents with varying ratios (100:0, 95:5, 90:10, 85:15, 80:20, 75:25, 70:30, 60:40, 50:50). Through this chromatographic separation, eight significant fractions were obtained. Among these fractions, fraction 5, eluted with hexane-ethyl acetate in an 80:20 ratio, was chosen based on thin-layer chromatography (TLC) analysis. Fraction 5 was subjected to multiple rounds of column chromatography on a silica gel bed (60-120 mesh size, Merck India) using hexane-ethyl acetate (80:20) as the elution solvent. Through this purification process, pure oleanolic acid was obtained with a yield of 1.85%, as verified by the presence of a single spot in TLC.

Subsequently, the isolated oleanolic acid underwent re-crystallization in methanol (MeOH), leading to the isolation of pure oleanolic acid.

3.4.2 Molecular Docking Assessment

Molecular docking was employed to enhance the understanding of ligand interactions, utilizing Auto Dock Vina (146). Preparation of proteins and ligands was conducted with the assistance of ADT tools. Initially, ligands underwent energy minimization using Chem 3D tools. Water molecules were removed, AD4-type atoms were assigned, and polar hydrogen atoms were added. 2D and 3D interactions were generated using Biovia Discovery Studio 2021(147). An *in silico* molecular docking approach was utilized to investigate the interactions with proteins such as albumin, beta-lactoglobulin, and lactoferrin.

3.4.3 Preparation of TPGS-SA

TPGS was modified with a carboxyl group through an esterification reaction with succinic anhydride (SA), catalyzed by dimethylamino pyridine (DMAP), resulting in TPGS-SA. In this process, 1 mmol (0.77 g) of TPGS and 2 mmol (0.10 g) of succinic anhydride were combined with a catalytic amount of DMAP (1 mmol) and stirred at 100 ºC under inert conditions for 24 hours. The reaction mixture was cooled to room temperature and precipitated using cold diethyl ether at -5 ºC, allowing it to settle overnight. The precipitated product was then agitated in dichloromethane (DCM), and any unreacted succinic anhydride was removed through repeated filtration. Finally, the white precipitate of TPGS-SA was obtained and subjected to vacuum drying. Following its use, it was stored at -20 ºC (148).

3.4.4 Characterization of TPGS-SA

The TPGS-SA preparation was verified through Mass spectrometry analysis. Mass spectra were obtained by dissolving TPGS and TPGS-SA in methanol and utilizing the SCIEX X500r Q-TOF, a High-Resolution mass spectrometry instrument. ^{1}H NMR spectra of both TPGS and TPGS-SA were also recorded using a BRUKER BioSpin International 500 MHz NMR

spectrometer. Chemical shift measurements were referenced to the internal standard, tetramethyl silane (TMS), and the samples were dissolved in deuterated DMSO-d^6 solvent.

3.4.5 Synthesis of non-targeted and CTX-conjugated OLA-loaded ALB-NPs

The synthesis of OLA-ALB-NPs utilized the emulsion-solvent evaporation method (149). The specified components are outlined in Table 4. In a nutshell, 5 mg of OLA was dissolved in a solution containing ethanol and chloroform in a 1:4 ratio. Concurrently, 30 mg of ALB was dissolved in 5 mL of deionized water. To this ALB solution, either TPGS (20 mg) or a combination of TPGS (10 mg) and TPGS-SA (10 mg) were introduced. The previously mixed ALB solution was stirred, and the OLA solution prepared earlier was added to it, allowing it to stir at 500 rpm for 15 minutes. Subsequently, the reaction mixture underwent 5 minutes of sonication using a probe sonicator. The solvent was removed from the synthesized OLA-loaded albumin nanoparticles (OLA-ALB-NPs) through the use of a rotary evaporator. The resulting nanoparticle dispersion was then filtered through a 0.22 μm PVDF filter to achieve uniform particle sizes. The targeted nanoparticles were created by forming a -CONH- linkage, covalently connecting the activated -COOH group on the nanoparticle surface with the -NH_2 of CTX in the presence of NHS and EDC. In the CTX-OLA-ALB-NPs preparation process, EDC and NHS were introduced to the stirred solution of NPs incorporating TPGS-SA in a molar ratio of 5:1. This mixture was stirred for 45 minutes. Subsequently, Cetuximab (2.5 mg) was added to this reaction mixture and stirred for 30 minutes. The formulated nanoparticle suspension was dialyzed against a saturated OLA solution using a one KDa dialysis membrane to eliminate any unreacted reagents. A similar procedure and composition were employed for the production of both non-targeted and targeted nanoparticles, excluding OLA in the latter case. During the preparation, C6 was used as a substitute for OLA. The cellular uptake study was conducted using both C6-free and C6-loaded formulations. Finally, after filtration through

a 0.22 µm syringe filter, large particles were separated from the nanoparticle formulations by centrifugation at 8000 rpm for 15 min.

Furthermore, to conduct an *in vivo* study targeting lung cancer, nanoparticles loaded with methylene blue (MB) were prepared using the procedure described earlier. In summary, 0.3 mg of MB was employed in lieu of OLA and the other components, and the process was executed as outlined above.

Table 4 Formulation of targeted and non-targeted ALB-NPs.

Batches	ALB (mg)	TPGS (mg)	TPGS-SA (mg)	OLA (mg)	CTX (mg)	C6 (mg)	MB (mg)
OLA-ALB-NPs	30	20	-	5	-	-	-
CTX-OLA-ALB-NPs	30	10	10	5	2.5	-	-
C6-ALB-NPs	30	20	-	-	-	0.3	-
CTX-C6-ALB-NPs	30	10	10	-	2.5	0.3	-
MB-ALB-NPs	30	20	-	-	-	-	0.3
CTX-MB-ALB-NPs	30	10	10	-	2.5	-	0.3

OLA-ALB-NPs: Oleanolic acid loaded ALB-NPs.
CTX-OLA-ALB-NPs: Oleanolic acid loaded CTX conjugated ALB-NPs.
C6-ALB-NPs: Coumarin-6 loaded ALB-NPs.
CTX-C6-ALB-NPs: Coumarin-6 loaded CTX conjugated ALB-NPs.
MB-ALB-NPs: Methylene blue loaded ALB-NPs.
CTX-MB-ALB-NPs: Methylene blue loaded CTX conjugated ALB-NPs.

3.5 Characterization of ALB-NPs

3.5.1 Surface charge, particle size, and polydispersity index of ALB-NPs

The zeta potential, polydispersity index (PDI), and hydrodynamic particle size of ALB-NPs were examined at room temperature using dynamic light scattering with a zeta sizer (Nano ZS 90, Malvern Instruments, UK). Prior to conducting any tests, the ALB-NPs were appropriately diluted in ultrapure water (150).

3.5.2 FTIR analysis

To examine chemical functionality and potential interactions among OLA, ALB, TPGS, and CTX, an FTIR spectrometer (Nicolet™ iS™ 5 spectrometer, Thermo Fisher Scientific, USA) was employed. Pure OLA, excipients, and the prepared nanoparticles were individually mixed with potassium bromide (KBr) to create the required pellets. Thin, transparent pellets were prepared using a hydraulic press with a force of 15.0 tons. Each pellet was subjected to separate infrared scans within the range of 4000 to 500 cm^{-1} (151).

3.5.3 X-Ray Diffraction (XRD) studies

The analysis of the crystalline structure of the drug, excipients, and nanoparticles was carried out using XRD analysis. The diffractogram of OLA, ALB, OLA-ALB-NPs, and CTX-OLA-ALB-NPs was obtained by employing the Bench Top X-Ray Diffraction system from Rigaku, Japan. X-ray scanning was performed on samples within the angular range of $2\theta = 10^{o}$ to $2\theta = 100^{o}$, utilizing a Cu Kα radiation source with a wavelength (λ) of 1.54 Å. A scan speed of 10^{o}/minute and a tube voltage of 40 KV were utilized (152).

3.5.4 SDS-PAGE analysis

This study employed SDS-PAGE to confirm the presence of bands corresponding to ALB, CTX, OLA-ALB-NPs, and the conjugation of CTX to CTX-ALB-NPs. Electrophoresis was conducted using a Vertical Mini Gel System vertical electrophoresis apparatus (Biorad, India) in a buffer solution containing 10% SDS, 1.92 mM glycine, and 0.25 mM Tris buffer at a pH of 8.2. The electrophoresis procedure followed a consistent voltage protocol, beginning with a voltage of 75 V for 30 minutes during the first phase, followed by a second phase at 115 V for 90 minutes. To visualize the gel, it was stained with Coomassie blue dye for 60 minutes. Excess stain was removed by rinsing the gel with a de-staining solution consisting of 50% water, 10% acetic acid, and 40% methanol (153).

3.5.5 Morphological analysis of ALB-NPs

3.5.5.1 Transmission electron microscopy

To characterize the size, shape, and morphology of OLA-ALB-NPs and CTX-OLA-ALB-NPs, HR-TEM (High-Resolution Transmission Electron Microscopy) analysis was conducted using equipment from FEI Pvt. Ltd., USA. Both nanoformulations of ALB-NPs were first appropriately diluted in deionized water and subjected to 10 minutes of sonication before analysis. Carbon-coated TEM grids were then spotted with a drop of the diluted ALB-NPs and left to dry at 40 ºC overnight. Additionally, Selected Area Electron Diffraction (SAED) analysis of the samples was carried out to assess the crystalline or polycrystalline nature of ALB-NPs (154).

3.5.5.2 Atomic force microscopy (AFM)

The topographical examination of OLA-ALB-NPs and CTX-OLA-ALB-NPs was conducted using the INTEGRA Prima AFM system. The ALB-NPs were suitably diluted with HPLC-grade water to prepare for AFM analysis and then sonicated for 10 minutes. Before the AFM analysis, a droplet of each OLA-ALB-NPs and CTX-OLA-ALB-NPs suspension was applied to separate glass slides measuring 2 x 2 cm, and these slides were vacuum-dried for 12 hours. The AFM images in both 2D and 3D were obtained for the ALB-NPs using NOVA and NT-MDT software (155).

3.5.6 Surface chemistry (XPS)

The surface analysis of OLA-ALB-NPs and CTX-OLA-ALB-NPs was conducted using the K-Alpha XPS system from Thermo Fisher Scientific, USA, which examined binding energies ranging from 100 to 800 eV. Prior to XPS analysis, ALB-NPs were deposited onto a glass slide measuring 1 x 1 cm and subjected to extended drying under vacuum conditions (156).

3.5.7 Entrapment efficiency

An HPLC analysis, using equipment from Shimadzu, Japan, was employed to determine the entrapment efficiency (EE) of OLA-ALB-NPs and CTX-OLA-ALB-NPs. In summary, 500 µL of the ALB-NPs was evaporated in a round-bottom flask through rotary evaporation. The resulting dried content of ALB-NPs was then reconstituted, mixed with methanol via vortexing, and centrifuged at 5,000 rpm for 20 minutes before further drying with a rotary evaporator. An HPLC method was established utilizing a mobile phase consisting of a methanol (MeOH)/water (H_2O) system in a 50:50 ratio. A calibration curve was created to quantify the concentrations of OLA, spanning concentrations from 10 to 10,000 ng/mL, based on peak area. The resultant curve displayed near-linearity (with a regression coefficient of 0.998). The percentage of OLA entrapped within the ALB-NPs was calculated by dividing the amount of OLA loaded by the initial amount of OLA taken up by the nanoparticles (157).

$$EE\%(w/w) = \frac{Amount\ of\ Oleanolic\ acid\ entrapped\ within\ nanoparticles}{Total\ amount\ of\ Oleanolic\ acid\ added\ to\ the\ formulation} \times 100$$

The entrapment efficiency of C6-loaded ALB-NPs was assessed using the same method outlined earlier. In summary, 30 µL of ALB-NPs was evaporated in a rotary evaporator, and then 70 µL of ethanol was introduced. This mixture was subsequently combined with 1 mL of distilled water and passed through a 0.22 µm syringe filter. To be concise, 200 µL of the resulting filtrate was loaded into a 96-well plate in triplicate, and the fluorescent intensity was measured to quantify the C6 content. Measurement was conducted at excitation and emission wavelengths of 457 nm and 502 nm, respectively, using a microplate reader (SpectraMax M series, Molecular Devices, USA).

3.5.8 Thermal analysis of ALB-NPs

3.5.8.1 Differential Scanning Calorimetry

The DSC-60 Plus equipment from Shimadzu Asia Pacific Pvt. Ltd. was utilized to assess the thermal compatibility of OLA with ALB and TPGS. In a nutshell, OLA, ALB, TPGS, a physical mixture of OLA and ALB, lyophilized OLA-ALB-NPs, and CTX-OLA-ALB-NPs were placed in standard aluminum pans, with an empty aluminum pan serving as the reference. The analysis was carried out over a temperature range of 25 ºC to 400 ºC, with a heating rate of 10 ºC per minute (158).

3.5.8.2 Thermogravimetric Analysis

To assess the thermal stability of ALB, OLA, TPGS, OLA-ALB-NPs, and CTX-OLA-ALB-NPs, a TGA-50 thermogravimetric analyzer from M/s Shimadzu Asia Pacific Pvt Ltd., Japan was employed. The samples were subjected to heating from 25 ºC to 800 ºC, with a heating rate of 10 ºC per minute, while dry nitrogen flowed through the experiment at a rate of 100 mL/min (159).

3.6 *In vitro* studies

3.6.1 *In vitro* release study

The OLA release profile from ALB-NPs was analyzed using the dialysis bag diffusion method. An airtight dialysis bag with a molecular weight cutoff of 1 KDa was filled with an equivalent volume of nanoparticles, equivalent to 0.3 mg of OLA-ALB-NPs. This sealed bag was then immersed in a 50 mL beaker containing either acetate buffer at pH 5.5 or PBS at pH 7.4. Water bath shakers from Remi Elektrotechnik Limited, Mumbai, were utilized to agitate the setup. 1 mL samples were collected at regular intervals, and fresh medium was replenished.

Before analysis, the samples were filtered through a 0.22 µm syringe filter, and OLA was extracted using 1 mL of ethyl acetate. Subsequently, all samples were vortexed, filtered to separate ethyl acetate, and allowed to evaporate. The dried product was then diluted with a mobile phase of methanol: water (50:50, 90 µL) prior to HPLC analysis. A graph illustrating the cumulative drug release over time was constructed (160).

3.6.2 *In vitro* hemocompatibility study

A hemolysis assay was conducted to assess the biocompatibility of ALB NPs and ensure their safety. Blood was sourced from a blood bank, and then it was subjected to centrifugation at 1000 rpm for 10 minutes to separate the red blood cells (RBCs). The supernatant was removed, and the RBCs were washed three times with PBS. A 2% v/v RBC solution in PBS was prepared, and 100 µL of this solution was combined with 100 µL of both OLA and OLA-loaded ALB NPs, along with 800 µL of saline as a diluent. This mixture was subsequently incubated at 37°C for 1 hour and then centrifuged at 1000 rpm for 5 minutes. Afterward, 200 µL of the supernatant was transferred to a 96-well plate.

Negative control samples contained 0.01 M PBS at pH 7.4, while positive control samples contained distilled water in the same quantity of 100 µL along with RBCs. The absorbance of the samples was measured at 540 nm using a microplate reader (161). Hemolysis was calculated using the following formula;

$$Hemolysis\ (\%) = \frac{Absorbance\ (test - negative\ control)}{Absorbance\ (positive\ control - negative\ control)} \times 100$$

3.6.3 Cell line maintenance and cell culture growth conditions

Cell lines were cultured in a humidified environment containing 5% CO_2 and 95% relative humidity. They were maintained in DMEM supplemented with 10% FBS, and a solution of penicillin-streptomycin conjugated with amphotericin B at a concentration of 100 IU/mL. The

cells were grown as monolayers and were detached into a single-cell suspension using 0.25% (w/v) trypsin/EDTA (1 mM).

3.6.4 *In vitro* cytotoxicity study

The cytotoxicity of pure OLA, OLA-ALB-NPs, CTX-OLA-ALB-NPs, and standard docetaxel on A549 and HEK-293 cells was evaluated using the MTT assay. Cells were seeded at a density of $1x10^4$ cells per well in DMEM and incubated for 24 hours at 37 ºC in a humidified incubator with 5% CO_2. After removing the culture medium, the cells were exposed to the specified samples in DMEM for 24 hours at concentrations ranging from 0.1 to 100 µg/mL. Subsequently, in each well, 90 µL of fresh medium was mixed with 10 µL of MTT solution (5 mg/mL in PBS, pH 7.4) at the designated time point. After 4 hours, the medium was gently aspirated to avoid disturbing the formazan crystals. Then, 100 µL of DMSO was introduced into each well and allowed to incubate for 30 minutes to dissolve the crystals. Absorbance at 570 nm was measured using a microplate reader (Spectramax Multiplate Reader, Molecular Devices, USA), and the percentage of viable cells was calculated in comparison to untreated cells using the following formula (162):

$$Cell\ viability\ (\%) = \frac{Absorbance\ of\ sample}{Absorbance\ of\ control} \text{ x } 100$$

3.6.5 Qualitative cellular uptake analysis

The cellular uptake of C6-loaded ALB-NPs by A549 cells was visualized using fluorescence microscopy. Cells were seeded in 12-well plates at a density of 5×10^4 cells per well and allowed to grow for 24 hours. Subsequently, DMEM containing free C6 and C6-loaded ALB-NPs at a concentration of 5 µg/mL was added to the wells and incubated for 12 hours at 37 ºC. The cells were then fixed with a 4% formaldehyde solution for 15 minutes. Next, the cell nuclei were labeled with DAPI. After removing the DAPI-containing medium, the cells were washed with a phosphate buffer. Fluorescence images were captured in the blue channel (DAPI) and

green channel (C6) at respective wavelength ranges of 340 nm and 488 nm. The internalization of NPs into the cytoplasm of A549 cells was quantified using the Image-J software, and an increase in the percentage of green signals indicated the cellular uptake of NPs (163).

3.6.6 Quantitative cellular uptake by flow cytometry

A549 cells were grown in 6-well plates at a seeding density of 1×10^5 cells per well. The culture medium used was DMEM supplemented with 10% FBS. The cells were then incubated at 37 ºC in an environment containing 5% CO_2 for 24 hours. Subsequently, the culture medium was replaced with 500 µL of serum-free DMEM containing either C6 as a control or C6-loaded ALB-NPs (C6-ALB-NPs and CTX-C6-ALB-NPs) at a coumarin-6 concentration of 5 µg/mL. The samples were then incubated at 37 ºC for 6 hours, after which they were appropriately prepared for flow cytometry analysis.

The cells underwent three rounds of rinsing with PBS, followed by trypsinization, collection, and centrifugation at 1000 rpm for 5 minutes. The supernatant was discarded, and the pellet was resuspended in 200 µL of phosphate-buffered saline. Data from 10,000 events were collected using an acquisition gate and subsequently analyzed using a Beckman Coulter CytoFlex flow cytometer (Becton Dickinson). The data were processed and analyzed with the CytExpert software (Dickinson-BD, USA) (164).

3.6.7 Apoptosis detection by Acridine orange/ethidium bromide staining

The assessment of cytotoxicity induced by ALB-NPs in A549 cells was further supported by an examination of the morphology of cancer cells following incubation with ALB-NPs and OLA control. Apoptosis, a natural process in living cells, is a crucial regulator in developing multicellular organisms. To differentiate between live and dead cells based on membrane integrity, a dual staining method with acridine orange (AO) and ethidium bromide (EtBr) was employed. Apoptosis and necrosis can be identified by observing changes in cell shape and chromatin structure (165). Live and dead cells were discerned through the staining process:

AO, which can permeate the plasma membrane, resulted in green fluorescence emitted from the nuclei, staining both live and dead cells. On the other hand, EtBr only stained dead cells in cases where the plasma membrane integrity had been compromised, emitting red-orange fluorescence from the DNA (166). In summary, A549 cells were seeded at a density of 1×10^5 cells per well in 12-well tissue culture plates and incubated for 24 hours in a 5% CO_2 environment with humidity. Subsequently, these A549 cells were exposed to OLA, OLA-ALB-NPs, and CTX-OLA-ALB-NPs at a concentration of 4.35 µg/mL for 24 hours in the CO_2 incubator. Following this incubation, the cells were washed with PBS at a pH of 7.4 and stained with solutions of AO and EtBr at a concentration of 40 µg/mL for 30 minutes. The cells were then rinsed with PBS, and morphological alterations were observed using an inverted fluorescent microscope with both red and green channels (167).

3.6.8 ROS generation assay

The assessment of the level of reactive oxygen species (ROS) was conducted using the cell-permeable probe 2′,7′-Dichlorofluorescin diacetate (DCFH-DA) (168). Elevated levels of intracellular ROS can potentially result in damage to the mitochondrial membrane, apoptosis, and eventual cell death. The impact of ALB-NPs on the formation of intracellular ROS in A549 cells was explored utilizing a peroxide-sensitive fluorescent dye, 2′,7′-Dichlorofluorescin diacetate (DCFH-DA). DCFH-DA is initially a non-fluorescent dye that can enter cells, and within the cytosol, it becomes oxidized by intracellular esterases, converting into the green fluorescent compound DCF, which remains confined within the cell. A549 cells were seeded at a density of 5×10^4 cells per well in 12-well culture plates and incubated at 37 ºC for 24 hours. Subsequently, these A549 cells were exposed to OLA, OLA-ALB-NPs, and CTX-OLA-ALB-NPs at concentrations equivalent to the IC_{50} value of the targeted nanoparticles for a duration of 24 hours. Following this treatment, the cells were washed with PBS at pH 7.4 and then incubated with 10 µM DCFH-DA for 30 minutes at 37 ºC in the absence of light. The

incubated samples were then examined under a fluorescence microscope, where the fluorescence from dichlorofluorescin (DCF) was observed and captured in the GFP channel (169).

3.6.9 AnnexinV- Alexa Fluor 488/propidium iodide staining assay

The extent of apoptosis in A549 cells was assessed using Annexin V-Alexa Fluor 488 and Propidium Iodide (PI) staining, and flow cytometry was employed with the Invitrogen™ Dead Cell Apoptosis Kits from ThermoFisher Scientific (170). A549 cells were seeded in 6-well culture plates at a density of 1×10^5 cells per well and cultured for 24 hours. After this incubation period, the cells were treated for 24 hours with OLA, OLA-ALB-NPs, and CTX-OLA-ALB-NPs at a concentration of 4.35 µg/mL.

Following treatment, the cells were harvested, washed with cold phosphate-buffered saline (PBS), centrifuged, and then resuspended in 1x annexin-binding buffer. Subsequently, 5 µL of Annexin V-Alexa Fluor solution and 1 µL of PI solution (at a working concentration of 100 µg/mL) were sequentially added to every 100 µL of the cell suspension. The cells were incubated in the dark for 15 minutes before being mixed with 1X annexin-binding buffer and kept on ice. Cell apoptosis was analyzed using flow cytometry (BD FACS Calibur, USA), and the data were presented as a dot plot showing Annexin V-Alexa Fluor against PI with quadrant gating.

3.6.10 Cell cycle analysis

One of the strategies for cancer treatment involves the use of anticancer drugs to arrest the cell cycle at specific phases. To determine which phase of the cell cycle is affected by the synthesized OLA-ALB-NPs and CTX-OLA-ALB-NPs, a cell cycle analysis was conducted. A549 cells were initially seeded in 6-well culture plates at a density of 1×10^5 cells per well and allowed to culture for 24 hours.

Following this, the cells were treated with OLA-ALB-NPs and CTX-OLA-ALB-NPs at a concentration of 4.35 µg/mL for 24 hours. The cells were subsequently washed with PBS, harvested in 1 mM EDTA (pH 7.4), and fixed with 75% ice-cold ethanol, keeping them at -20 ºC overnight. After another wash with PBS, the cells were centrifuged and stained with a solution containing 20 µg/mL PI (from Sigma Aldrich, USA), 100 µg/mL RNase A (at 10 mg/mL), and 0.1% triton-X in phosphate-buffered saline. The staining occurred for 30 minutes at 37 ºC. Cell samples were then analyzed for cell cycle phases using a flow cytometer after a 30-minute incubation at 37 ºC in the dark (BD FACS Calibur, USA) (171).

3.7 *In vivo* studies

3.7.1 Pharmacokinetic study

Wistar rats, aged 4-5 weeks and weighing 150-200 grams, were obtained and housed in a controlled environment with regulated climate and humidity. They were subjected to a 12-hour light/dark cycle at room temperature. The rats were randomly divided into four separate groups, each consisting of four rats. The control group received an intravenous (tail vein) injection of saline only, while the standard group was administered OLA at a dose of 10 mg/kg. Similarly, the other two groups were treated with distinct ALB-NPs at equivalent concentrations.

Before collecting blood samples, the rats were anesthetized. Blood samples of 500 µL were collected at time intervals of 0, 1, 2, 4, 8, 12, and 24 hours through the retro-orbital plexus and placed in Eppendorf tubes containing a 3.8% w/v sodium citrate solution. Subsequently, the samples were centrifuged at 3,000 rpm for 10 minutes. To extract the drug, 200 µL of plasma was vortexed and transferred to vials containing 1 mL of ethyl acetate. The ethyl acetate was pipetted out and left for complete evaporation. After vortexing and filtration, 100 µL of filtered mobile phase (consisting of methanol and water in a 50:50 ratio) was added to the dried ethyl acetate residues and placed into HPLC vials. An OLA calibration curve was established for plasma using stock solutions ranging from 10 ng/mL to 1000 ng/mL.

To assess the OLA content in plasma samples, RP-HPLC with a C18 column (250 mm x 4.6 mm, 5 µm particle size) composed of octadecylsilane (ODS) was employed. The mobile phase used had a flow rate of 1 mL/min and consisted of a 50:50 mixture of methanol and water. A PDA detector (SPD-M40 PDA detector with 1024 diodes) was utilized to monitor the samples at a wavelength of 206 nm. Following the injection of 10 µL of each sample into the HPLC column, the concentration was determined using the standard OLA calibration curve equation. To evaluate the pharmacokinetic characteristics of OLA in various ALB-NPs, a graph depicting the plasma concentration of the drug over time was created. Pharmacokinetic parameters were subsequently determined using Kinetica® software (163).

3.7.2 Histopathology

A histopathological examination was carried out to assess potential adverse effects on Wistar rats following the administration of OLA, non-targeted ALB-NPs, and targeted ALB-NPs. The rats were randomly divided into four groups, each consisting of four rats. The administration of ALB-NPs was done intravenously via the tail vein. These groups received injections as follows: saline control, OLA, OLA-ALB-NPs, and CTX-OLA-ALB-NPs, all at a dose of 10 mg/kg, administered once every three days for a total of three times (on the 3rd, 6th, and 9th day).

On the 15th day, the animals were humanely euthanized, and major organs such as the heart, kidneys, liver, and lungs were removed and rinsed with normal saline. These specimens were preserved in 10% formalin and subsequently embedded in paraffin. The 5 µm-thick paraffin sections were stained with hematoxylin and eosin. Brightfield microscopes, specifically Dewinter microscopes, were utilized to examine the histological findings in these specimen sections (172).

3.7.3 *In vivo* lung safety study in rats

The animals were randomly divided into four groups, consisting of three treatment groups (OLA, OLA-ALB-NPs, and CTX-OLA-ALB-NPs) and one control group, with each group containing 3 rats. This sample size of three rats per group was maintained for the 0th, 7th, and 15th day time points. Throughout the duration of the experiment, the daily health status of the rats was vigilantly monitored.

The control group of animals received a standard saline solution (0.9% NaCl) via intravenous (*i.v.*) administration. The other groups of animals were treated with OLA, OLA-ALB-NPs, and CTX-OLA-ALB-NPs, respectively. At the specified time intervals of 0, 7, and 15 days after the administration of the formulations, the rats were humanely euthanized using an intraperitoneal (*i.p.*) injection of urethane (1.5 g/kg for rats). Following the opening of the thorax, the lungs were perfused with normal saline at a dosage of 26.5 mL/kg for rats. Subsequently, the trachea was cannulated, and bronchoalveolar lavage (BAL) fluid was collected by instilling approximately 4 mL of normal saline into the lungs and then thoroughly rinsing. The BAL fluid was centrifuged at 400 ×g at 4 ºC for 10 minutes and stored at -20 ºC until further analysis.

All biochemical assays were performed on the BAL fluids, including the determination of LDH (Crest Biosystems, Goa, India) and ALP (Span Diagnostics Ltd., Surat, India), using the respective diagnostic kits following the manufacturer's instructions (173).

3.7.4 *In vivo* lung cancer targeting study by ultrasound and photoacoustic study

The work discussed in this study evaluates the distribution of methylene blue (MB) loaded nanoparticles in a mice lung cancer model (174) employing an ultrasound and photoacoustic imaging system (Vevo LAZR_X Vevo 3100 imaging system, Toronto, Canada). Cancer was induced in the experimental subjects using benzo(a)pyrene (B(a)P) (172). The experimental mice, which numbered three and were males, belonged to the Swiss albino strain and weighed

between 16-20 grams. These mice were maintained in a controlled environment with access to water and a standard rodent diet.

To anesthetize the animals, inhalation anesthesia with isoflurane was administered at a concentration of 3% for induction and 1.5-2% for maintenance. Subsequently, the animals were positioned in a supine posture on a heated operating table, and an ultrasonic transducer equipped with an optical fiber bundle was placed above the animals to capture clear parasternal long axis lung images. To ensure optimal imaging quality and eliminate air bubbles between the transducer and the animal's skin, a clear ultrasonic gel was applied. The imaging depth was consistently set at 18 mm for all scans. Photoacoustic (PA) signals were recorded both before and after the intravenous injection of MB control and MB-loaded nanoparticles (MB-ALB-NPs and CTX-MB-ALB-NPs). These injections were administered at 30-minute intervals through the tail vein. Data processing was carried out using VevoLAB software V.3.2.5.

To minimize the background PA signal from hemoglobin, an initial baseline PA signal was subtracted before the nanoparticles were introduced. The presence of nanoparticles in the lungs of the mice was visualized through photoacoustic images, with green signals representing the nanoparticles. Following the 30-minute intravenous administration, both ultrasound and photoacoustic imaging were conducted to examine the biodistribution of MB control, non-targeted, and targeted MB-loaded nanoparticles within the lung tissue of the mice (175).

3.8 Statistical analysis

A minimum of three independent experiments were carried out, and the outcomes were presented as the mean values along with their respective standard deviations. We employed GraphPad Prism version 5 for our statistical analysis. Statistical significance was assessed using one-way ANOVA, t-test, and Tukey's multiple comparison test. A p-value greater than or equal to 0.05 was considered statistically nonsignificant, while p-values less than 0.05 were

regarded as statistically significant, indicated by symbols (*, **, ***, and ****) corresponding to p-values less than 0.05, 0.01, 0.001, and 0.0001, respectively.

3.9 Results and discussion

3.9.1 *In silico* docking

In silico docking, experiments were conducted to investigate the suitability of different biodegradable proteins as carriers for OLA, as indicated in Table 5. Three specific biodegradable proteins, namely bovine serum albumin (4JK4), bovine beta-lactoglobulin (3NPO), and bovine lactoferrin (1BLF), were selected for this analysis. Fig. 12 illustrates the comparative binding affinities between OLA and these proteins, based on the various interactions observed.

Upon evaluating the binding energies, it was observed that albumin exhibited a more robust binding affinity with OLA, approximately -8.2 kcal/mol, in contrast to -7.5 kcal/mol for 3NPO and -6.2 kcal/mol for 1BLF among all the polymers considered.

An analysis of the 2D interactions between the ligand OLA and the protein 4JK4 showed that the methyl group of the ligand engaged in alkyl-alkyl interactions with ILE297 and ARG336 residues. Likewise, the cyclohexane and cyclohexene rings also formed alkyl-alkyl interactions with ARG336, HIS337, and LEU304 residues. Furthermore, the hydroxyl group of the carboxylic acid displayed conventional hydrogen bond interactions with PRO302 and LEU301 residues.

Table 5 Illustration of the interaction between ligand and protein

Ligand	Protein	Binding Energy (kcal/mol)	Interacting Amino acids
OLA	4JK4	-8.2	LEU301, PRO302, PRO303, LYS377, TYR333, PHE373, TYR340, ILE297, ARG336, HIS337, LEU304

OLA	3NPO	-7.5	LEU31, PRO38, VAL41, LEU39, LYS69, HOH1049, ILE71, ASN109, ASN88, ASN90, ALA86, ILE84
OLA	1BLF	-6.2	ASN476, ALA668, ALA590, LEU473, ILE469, LEU589, ASN667, ASN671, GLU664, TYR665

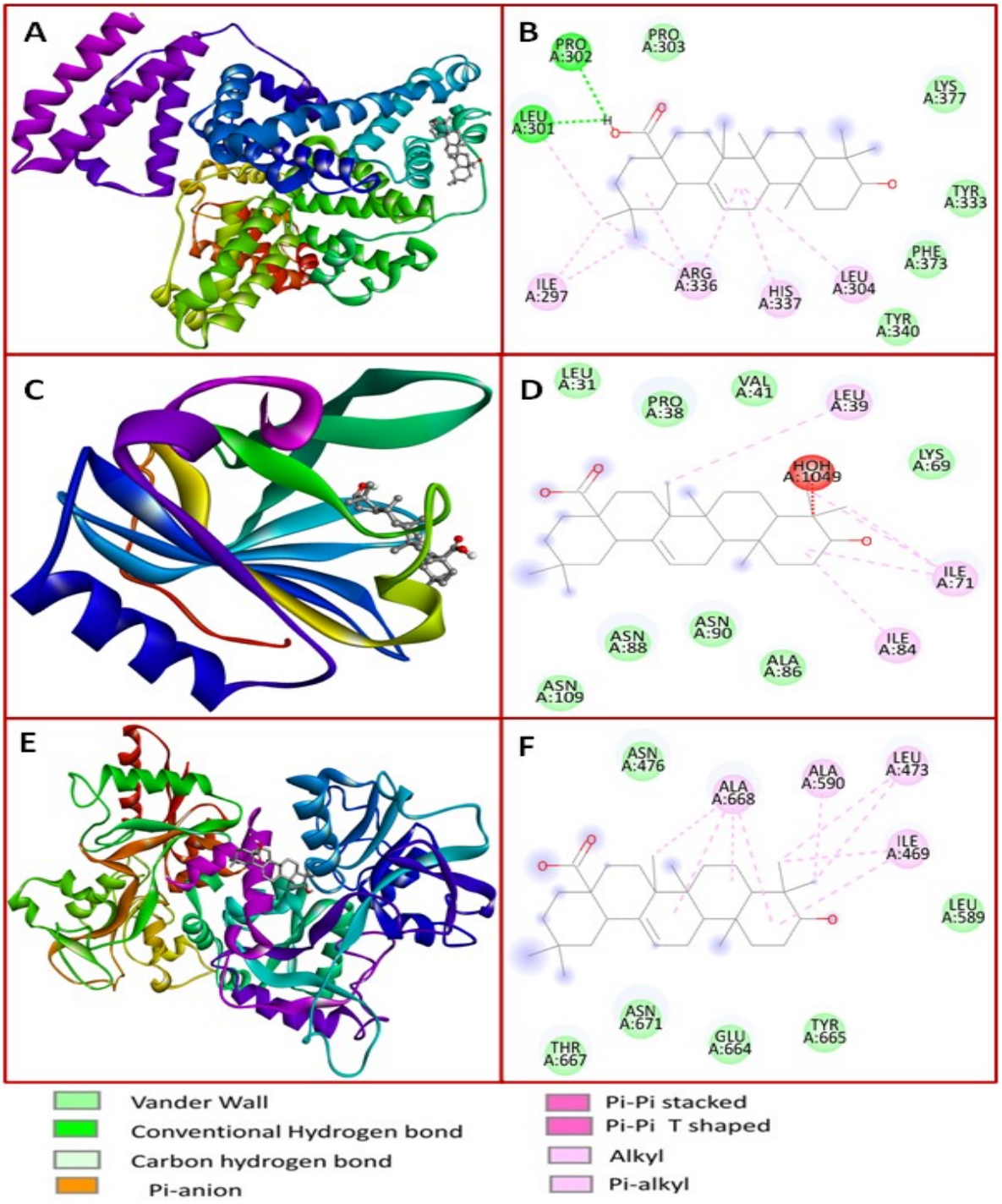

Figure 12 3D (A) and 2D (B) binding interaction of OLA against bovine serum albumin (4JK4); 3D (C) and 2D (D) binding interaction of OLA against bovine beta lactoglobulin (3NPO); 3D (E) and 2D (F) binding interaction of OLA against bovine lactoferrin (1BLF) respectively

3.9.2 Characterization of TPGS-SA

The HRMS spectra of both TPGS and TPGS-SA were analyzed to determine the mass of oligomeric adducts and their charge states. The sodium adduct formed by TPGS was identified as $C_{33}H_{54}O_5$-$(CH_2CH_2O)_n$ + Na. An increase of 101 Da in the TPGS-SA HRMS spectrum indicated a reaction between TPGS and succinic anhydride, confirming the interaction. The empirical formula [$C_{33}H_{54}O_5$-$(CH_2CH_2O)_n$] was proposed for various oligomers of TPGS-SA forming sodium adducts (CO-C_2H_4-COOH + Na). The spectra of both TPGS and TPGS-SA displayed oligomers in multiple charge states.

For instance, the reaction between TPGS oligomer with an n value of 25, [$C_{33}H_{54}O_5$-$(CH_2CH_2O)_n$] at 1630 Da (or m/z 1654 in sodium salt form), and succinic acid yielded a species at m/z 1755. Similar spectral patterns were observed when comparing TPGS and TPGS-SA. The HRMS data and ^{1}H NMR spectra confirmed the TPGS-SA structure, consistent with previously published literature.

In the ^{1}H NMR spectra of TPGS, signals corresponding to the ethylene protons of the PEG chain appeared at 3.5-3.6 ppm, while signals in the aliphatic region (1-3 ppm) were attributed to different protons of the vitamin E-tail. The ^{1}H NMR spectra of TPGS-SA exhibited similar signals to those of TPGS, with the addition of succinyl methylene (-CH_2) protons at 2.3 and 2.9 ppm, indicating the reaction between TPGS and succinic anhydride.

3.10 Characterization of Nanoparticles

3.10.1 Size, polydispersity, and zeta potential

The characteristics of ALB-NPs are outlined in Table 6. The hydrodynamic diameters of the prepared ALB-NPs ranged from 171 ± 4.8 nm to 180 ± 3.7 nm. Conjugating CTX to ALB-NPs significantly increased the particle size ($p < 0.05$). The zeta potential of OLA-ALB-NPs was -30.5 ± 2.8 mV, and this value changed to -33.3 ± 3.4 mV after cetuximab conjugation in CTX-OLA-ALB-NPs. The enhanced negative charge in CTX-conjugated ALB-NPs can be attributed

to the dominant anionic groups of CTX, causing the surface of the targeted NPs to become more negatively charged.

Table 6 Physicochemical parameters of prepared ALB-NPs

Batches	Particle Size (nm) (Mean ± SD*)	PDI (Mean ± SD*)	Zeta potential (mV) (Mean ± SD*)	Entrapment efficiency (%) (Mean ± SD*)
OLA-ALB-NPs	171 ± 4.8	0.14 ± 0.07	-30.5 ± 2.8	75.3 ± 5.1
CTX-OLA-ALB-NPs	180 ± 3.7	0.26 ± 0.03	-33.3 ± 3.4	71.5 ± 3.5
C6-ALB-NPs	162 ± 4.2	0.25 ± 0.06	-27.7 ± 4.2	73.8 ± 4.2
CTX-C6-ALB-NPs	177 ± 2.3	0.28 ± 0.09	-30.2 ± 3.2	68.6 ± 3.1
MB-ALB-NPs	155 ± 3.2	0.21 ± 0.03	-25.6 ± 3.1	62.4 ± 3.5
CTX-MB-ALB-NPs	174 ± 3.1	0.27 ± 0.04	-28.3 ± 1.9	63.2 ± 1.8

*n = 3; S.D: Standard deviation
OLA-ALB-NPs: Oleanolic acid loaded ALB-NPs
CTX-OLA-ALB-NPs: CTX conjugated Oleanolic acid loaded ALB-NPs
C6-ALB-NPs: Coumarin-6 loaded ALB-NPs
CTX-C6-ALB-NPs: Coumarin-6 loaded CTX conjugated ALB-NPs
MB-ALB-NPs: MB loaded ALB-NPs
CTX-MB-ALB-NPs: MB loaded CTX conjugated ALB-NPs

3.10.2 FTIR spectroscopy

FTIR spectral analysis was conducted on OLA, ALB, the physical mixture of OLA and CTX, OLA-ALB-NPs, and CTX-OLA-ALB-NPs. In the case of ALB, the distinctive peaks corresponding to primary amine stretching were observed at 3310 cm^{-1}. Additionally, three vibrational bands at 1657, 1541, and 1243 cm^{-1} were identified as ALB amide linkages (designated as amide I, II, and III). On the other hand, OLA exhibited specific peaks at 3457 cm^{-1}, 2944 cm^{-1}, and 1696 cm^{-1} in the FTIR spectrum, indicating O-H, C-H, and C=O stretching vibrations, respectively (Table 7). The peaks of OLA and ALB were less prominent in OLA-ALB-NPs and CTX-OLA-ALB-NPs compared to the physical mixture (ALB + OLA). This attenuation suggests the successful interaction of ingredients within ALB-NPs, as illustrated in Fig 13A.

Table 7 FTIR peak assignment of ALB, OLA, TPGS, CTX, OLA-ALB-NPs, CTX-OLA-ALB-NPs

Types of stretching & bending vibration	**Characteristic absorption bands/peaks ν_{max} cm^{-1}**					
	ALB	**OLA**	**TPGS**	**CTX**	**OLA-ALB-NPs**	**CTX-OLA-ALB-NPs**
O-H Stretching	-	3457 cm^{-1}	3428 cm^{-1}	3442 cm^{-1}	3854 cm^{-1}	3744 cm^{-1}
N-H Stretching	3310 cm^{-1} 3068 cm^{-1}	-	-	-	3451 cm^{-1}	3442 cm^{-1}
C-H Stretching	2961 cm^{-1}	2944 cm^{-1}	2870 cm^{-1}	2927 cm^{-1}	2930 cm^{-1}	2942 cm^{-1}
C=O stretching	1657 cm^{-1}	1696 cm^{-1}	1736 cm^{-1} 1643 cm^{-1}	1635 cm^{-1}	1636 cm^{-1}	1658 cm^{-1}
C–N stretching	1243 cm^{-1}	NA	NA	1238 cm^{-1}	1243 cm^{-1}	1249 cm^{-1}
N–H bending	1541 cm^{-1}	NA	-	1559 cm^{-1}	1563 cm^{-1}	1541 cm^{-1}
C-O stretching	1161 cm^{-1}	1039 cm^{-1}	1109 cm^{-1}	1053 cm^{-1}	1054 cm^{-1}	1068 cm^{-1}

3.10.3 XRD

Fig. 13B below illustrates the XRD overlay spectrum of OLA, ALB, OLA-ALB-NPs, and CTX-OLA-ALB-NPs. The XRD spectrum of pure OLA revealed distinct sharp peaks at 10.85, 12.91, 13.67, 15.74, 17.47, and 19.33º, indicating the drug's crystalline nature. In contrast, TPGS displayed two sharp characteristic peaks at 19.14 and 23.28º, alongside broad peaks, showcasing its semi-crystalline quality. ALB, on the other hand, exhibited broad peaks at approximately 20.82º, signifying its amorphous nature.

Notably, both OLA-ALB-NPs and CTX-OLA-ALB-NPs displayed a single sharp peak with lower intensity at 2θ of 25º. This peak was also observed in the spectra of TPGS, suggesting its presence on the surface. However, in CTX-conjugated NPs, the intensity of this TPGS peak was slightly reduced compared to non-targeted NPs, possibly due to the presence of CTX.

Moreover, the characteristic peaks of OLA were absent in the NP spectra, indicating its effective loading.

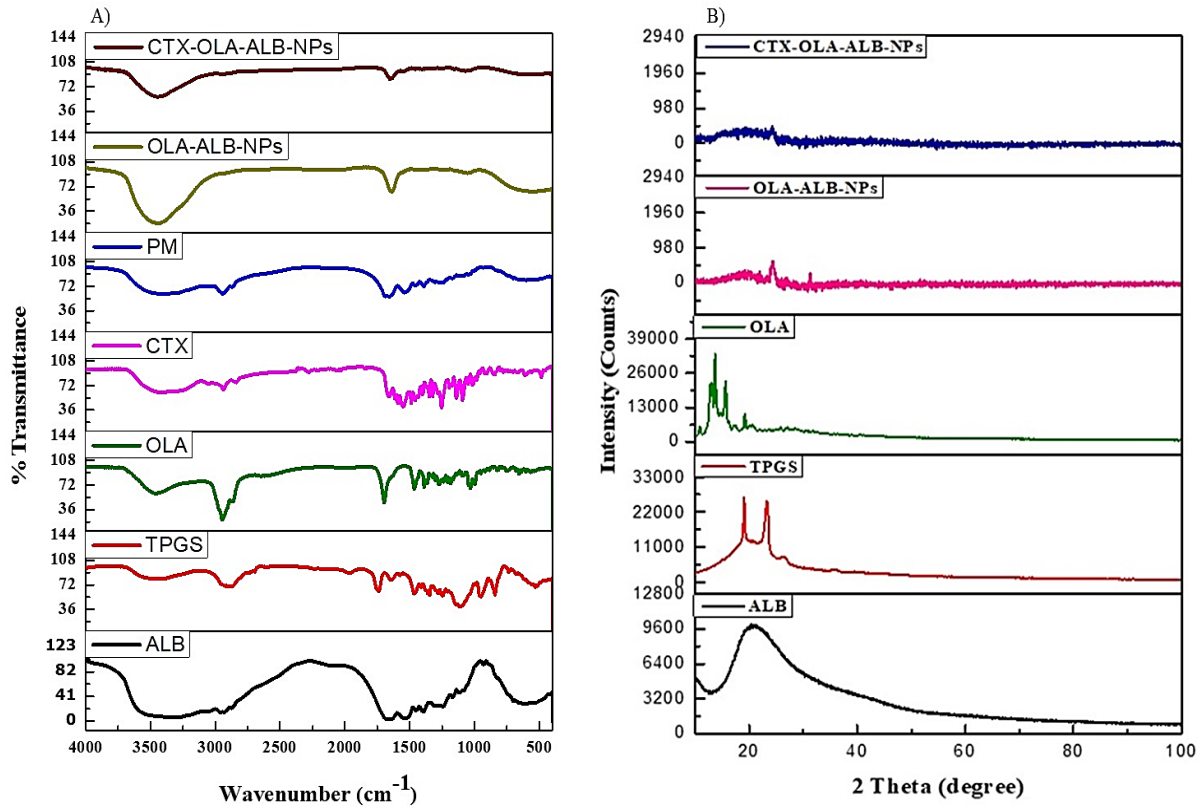

Figure 13 A) FTIR analysis drug, excipients and their physical mixture. B) XRD analysis of ALB, TPGS, OLA and non-targeted and CTX conjugated targeted ALB-NPs

3.10.4 SDS-PAGE analysis

In this study, we performed SDS-PAGE analysis on samples of pure ALB, CTX, OLA-ALB-NPs, and CTX-OLA-ALB-NPs. The experimental procedure involved the utilization of gel electrophoresis for the separation of bands based on their molecular weights. The outcomes of this investigation offer valuable insights into the molecular characteristics of CTX-OLA-ALB-NPs and contribute to a broader comprehension of the surface conjugation of CTX with OLA-ALB-NPs.

The results of this analysis revealed that pure CTX displayed two distinctive bands at 54 and 29 kDa, as illustrated in Fig. 14. In the case of CTX-OLA-ALB-NPs, two distinct bands were observed. These findings suggest that one of the bands corresponds to CTX, while the other

corresponds to ALB, providing evidence of the presence of CTX on the surface of ALB-NPs.ALB-NPs.

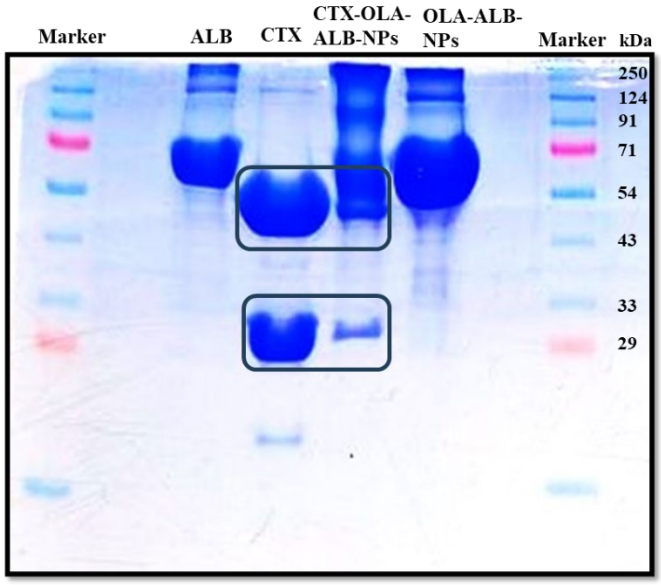

Figure 14 SDS-PAGE of pure ALB, pure CTX, CTX-OLA-ALB-NPs, and OLA-ALB-NPs showing confirmation of loading of CTX moiety with OLA-ALB-NPs. Polyacrylamide gels were stained with Coomassie Brilliant Blue

3.10.5 TEM

The ALB-NPs were appeared to be spherical and uniformly dispersed (Fig. 15A). Moreover, the physical state of ALB-NPs appeared in the TEM images, was assessed by the SAED study (Selected area electron diffraction). The corresponding SAED images demonstrated the diffused ring pattern indicating their amorphous nature (Fig. 15B).

3.10.6 AFM

The surface topology of ALB-NPs was investigated using AFM analysis. As displayed in the Fig. 15C and 15D, the surface of ALB-NPs appeared spherical in both 2-Dimensional and 3-Dimensional photographs of AFM.

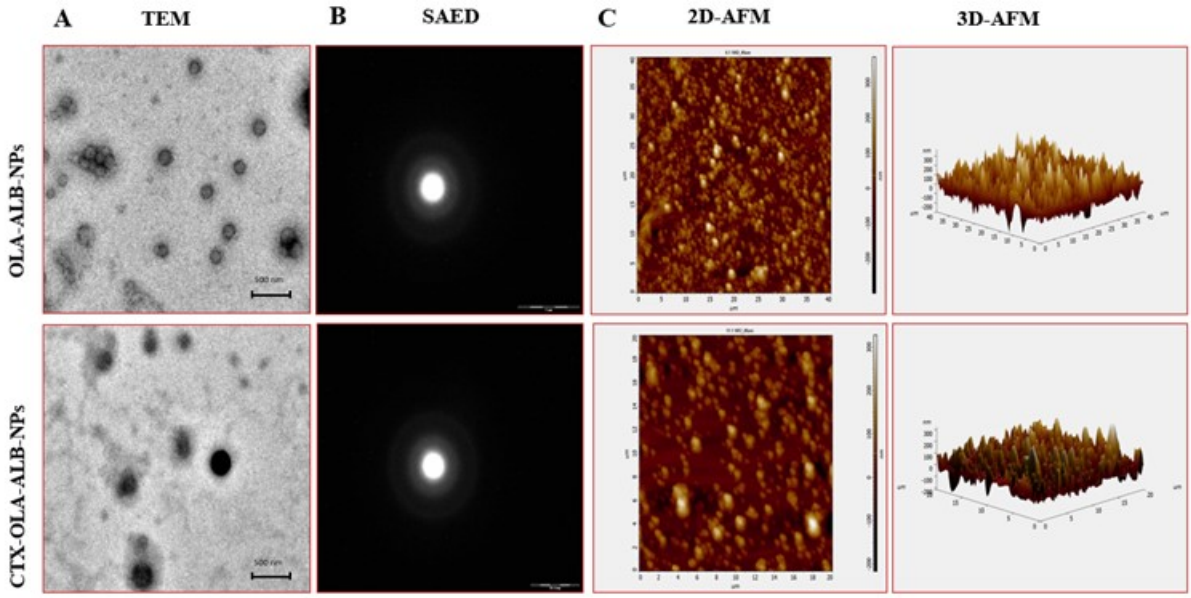

Figure 15 Morphological analyses of non-targeted and CTX conjugated ALB-NPs

3.10.7 XPS analysis

The acquired XPS spectra indicated the expected peaks for components C, N, and O, as shown in Fig. 16A and 16B. There were three peaks detected at binding energies of 290-280 eV, 404-395 eV, and 537-527 eV attributed to C 1s, N 1s, and O 1s, respectively. The histogram showing the atomic percentage of nitrogen demonstrated that the atomic percentage of N 1s was significantly higher in the CTX conjugated ALB-NPs. Since CTX has a considerable number of nitrogen-containing atoms in its chemical formula, the enhanced nitrogen percentage in CTX-OLA-ALB-NPs is evident in the conjugation of CTX in CTX conjugated ALB-NPs.

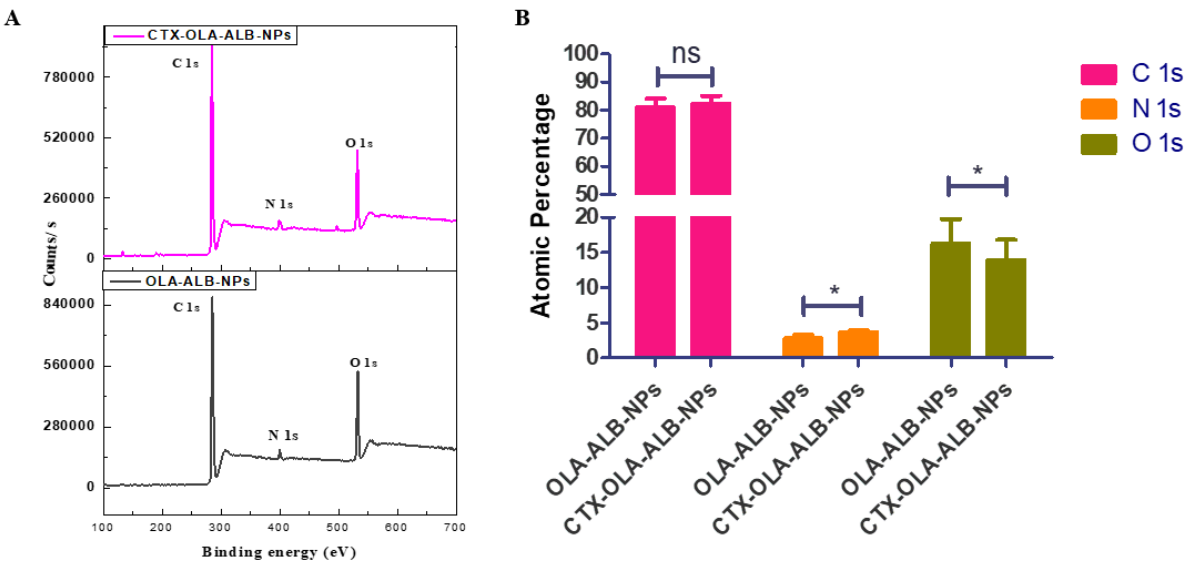

Figure 16 XPS analysis of non-targeted and CTX conjugated ALB-NPs. B) Histogram showing atomic percentage on nanoparticle surface

3.10.8 DSC analysis

The DSC curve of ALB showed characteristic endothermic peaks at 62.3 ºC, 217.9 ºC, 206.0 ºC, 291.2 ºC, 312.7 ºC, 338.7 ºC (Fig. 17A). Whereas, DSC curves of TPGS showed sharp endotherm at 36 ºC, indicating its melting point. The DSC curve of OLA, exhibited a sharp endotherm at 314.2 ºC, revealing its melting point. However, a small exothermic peak was also observed at 194.9 °C. The physical mixture of OLA and ALB showed a small endotherm related to the OLA, at the same temperature, which showed no chemical interaction. The non-targeted NPs displayed no characteristic peaks and demonstrated their good thermal stability. Whereas the CTX-targeted NPs exhibited several endothermic peaks at 53.4 ºC, 216.4 ºC, 304.5 ºC, 327.6 ºC. Since, the endothermic peak of OLA was missing in the both of the NP's formulations, which support its appropriate entrapment in the ALB matrix and therefore improve its thermal stability.

3.10.9 TGA analysis

Thermogravimetric analysis (TGA) was used to measure percent weight changes of ALB, OLA, TPGS, physical mixture and NPs as a function of temperature, which demonstrated their thermal stability and undesired physical or chemical interactions (Fig. 17B). The results depicted that there was no significant weight loss of ALB, OLA, TPGS, physical mixture and NPs up to 300 ºC. Whereas a slower degradation rate of ALB, OLA-ALB-NPs and CTX-OLA-ALB-NPs, after 300 ºC indicating its improved stability compared to OLA. However, the TGA curve of TPGS also showed faster degradation rate between 300 ºC to 400 ºC. Moreover, the TGA curve of physical mixture of ALB and OLA exhibited less percentage of weight loss, indicating its slow degradation. The TGA curve of TPGS and OLA demonstrated rapid weight loss between 300 to 400 ºC, whereas both the NPs demonstrated slower degradation /weight loss.

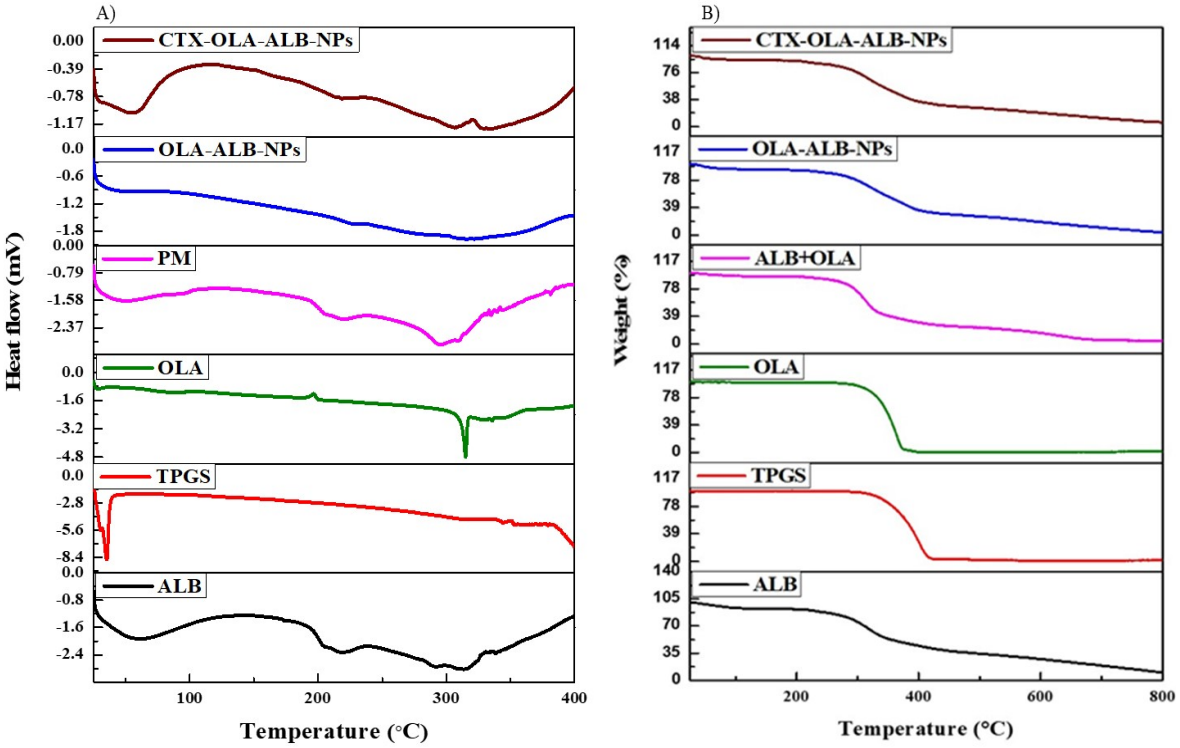

Figure 17 Thermal analysis A) DSC and B) TGA analysis of drug, polymer, excipients, their physical mixture and non-targeted and CTX conjugated ALB NPs

3.10.10 Entrapment Efficiency

The entrapment efficiency of OLA-ALB-NPs, CTX-OLA-ALB-NPs was 82.2 ± 3.9 % and 78.08 ± 2.3 % respectively (Table 6). The small drop of the OLA content in targeted NPs, may be due to the interference of the CTX conjugation on the surface. The entrapment efficiency of C6 and MB loaded NPs has been presented in the Table 6.

3.11 *In vitro* analysis

3.11.1 *In vitro* drug release

Fig. 19D shows the *in vitro* drug release analysis of OLA-ALB-NPs followed by a steady release lasting up to 72 h for CTX-OLA-ALB-NPs. Furthermore, OLA release was higher in PBS pH 5.5, possibly due to albumin denaturation and precipitation, whereas it was comparably lesser in PBS 7.4. The outcomes showed that increased OLA release from ALB-NPs in a cancer microenvironment (pH 5.5) may be advantageous for targeted delivery of OLA.

3.11.2 *In vitro* hemocompatibility study

The biocompatibility and safety of the OLA, OLA-ALB NPs, and CTX-OLA-ALB NPs were assessed in human blood. The hemolysis percentages of OLA, OLA-ALB NPs, and CTX-OLA-ALB NPs were determined to be 3.25 ± 0.18 %, 3.34 ± 0.90 %, and 3.10 ± 0.23 %, respectively. The experimental findings depicted in Fig. 18 demonstrated that all formulations of NPs did not cause hemolysis in human blood.

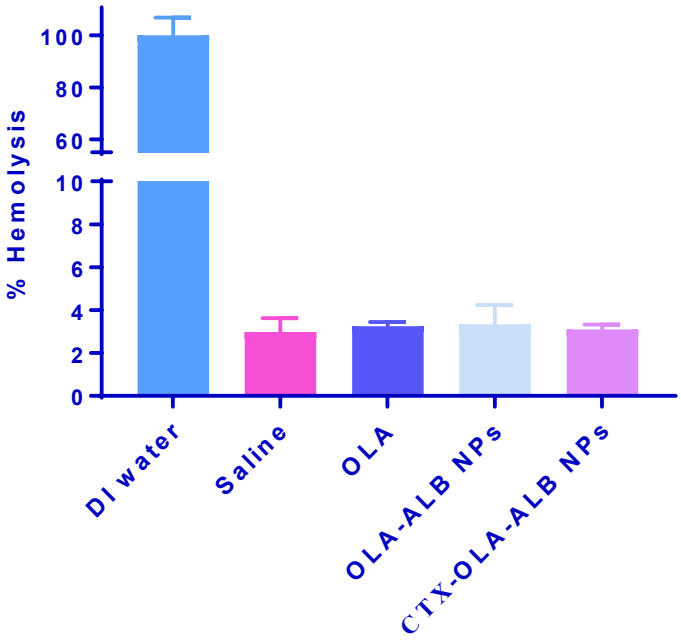

Figure 18 Hemocompatibility study of OLA, OLA-ALB NPs, CTX-OLA-ALB NPs

3.11.3 *In vitro* cytotoxicity study

The MTT test, a colorimetric assay, was employed in this study to assess cellular metabolic activity based on color intensity (176). The study evaluated the cytotoxic effects and efficacy of OLA, Docetaxel, and ALB-NPs on A549 cells. Additionally, the safety of prepared ALB-NPs on normal cells was tested using HEK 293 cells as a control. Fig 19A illustrates the outcomes of the MTT assay after 24 hours of treatment with OLA, Docetaxel, OLA-ALB-NPs, and CTX-OLA-ALB-NPs in A549 cells. Fig 19B presents the cytotoxic impact of these substances on normal (HEK 293) cells. After 24 hours of treatment, the IC_{50} values for Docetaxel (positive control), OLA control, OLA-ALB-NPs, and CTX-OLA-ALB-NPs in A549 cells were 25.3 ± 2.7 µg/mL, 98.21 ± 1.45 µg/mL, 13.87 ± 1.28 µg/mL, and 4.34 ± 1.90 µg/mL, respectively. The IC_{50} value of CTX-OLA-ALB-NPs was about 5 folds ($p < 0.001$), 23 folds ($p < 0.001$) and 3 folds ($p < 0.001$) lesser ($p < 0.001$) than docetaxel, OLA control and OLA-ALB-NPs which implies the cytotoxic potential of ALB-NPs towards A549 cell.

In contrast, the non-cancerous HEK-293 cell line exhibited significantly higher cell viability at approximately 75%. This suggests that OLA and OLA-loaded ALB-NPs might possess higher

selectivity for cancer cells while causing less harm to normal cells. When tested on the lung cancer cell line A549, CTX-OLA-ALB-NPs decreased cell viability and facilitated cellular internalization, indicating the cytotoxic nature of these nanoparticles. The study showed that this effect was concentration-dependent, with cell viability decreasing consistently as the concentration increased. Notably, ALB-NPs exhibited considerably higher cytotoxicity against malignant cells compared to control cells, suggesting their potential as effective anticancer agents in the future. Moreover, due to albumin's natural presence in the human body, ALB-NPs are considered safe and non-toxic for human consumption.

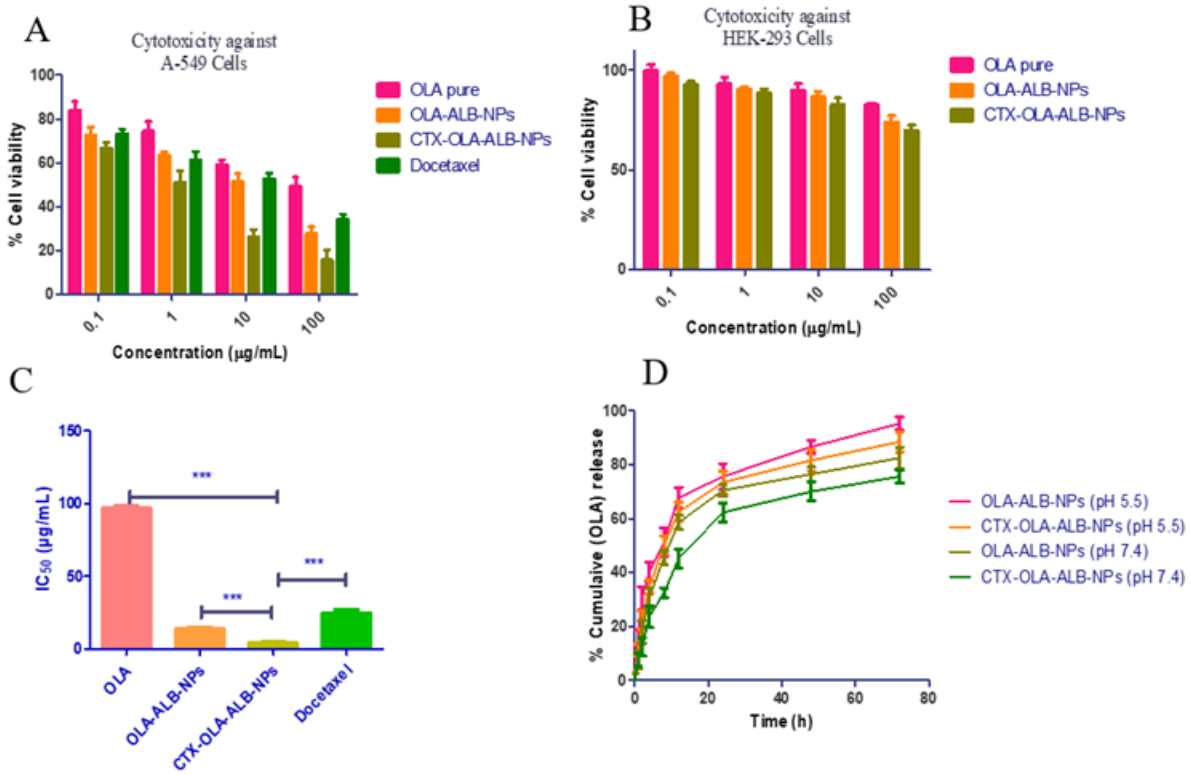

Figure 19 A) Cell-viability analysis of OLA, OLA-ALB-NPs, CTX-OLA-ALB-NPs and Docetaxel against A549 cancer cells and B) A) Cell-viability analysis of OLA, OLA-ALB-NPs, and CTX-OLA-ALB-NPs against HEK-293 cells. C) Statistical analysis among OLA, OLA-ALB-NPs, and CTX-OLA-ALB-NPs. D) *In vitro* drug release profile in pH 5.5 and 7.4

3.11.4 Qualitative cellular uptake study

The green channel shows C6-loaded NPs internalization, which was assessed using image-J software by measuring the percent intensity of green signals (Fig. 20A). As shown in the histogram, the percentage area of green channels in fluorescence pictures of CTX conjugated NPs was approximately 18 times and 4 times increased than that of C6 control ($p < 0.001$) and non-targeted NPs ($p < 0.001$) respectively (Fig. 20B). The result suggested that the increased uptake of CTX- conjugated NPs in A549 cells (EGFR positive) may be due to EGFR-mediated endocytosis.

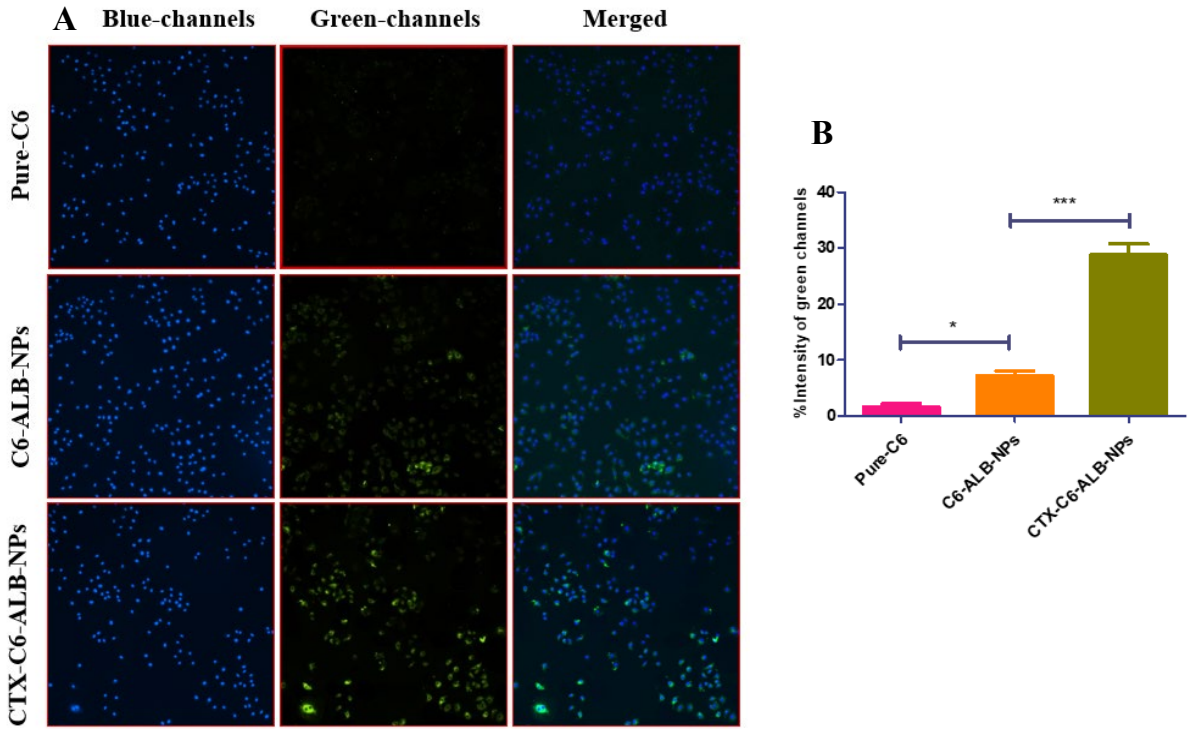

Figure 20 A) Cellular-uptake images of pure C6 and C6 loaded non-targeted and CTX conjugated ALB-NPs, and B) Percent intensity of green channels in cellular-uptake images

3.11.5 Quantitative cellular uptake study

Flow cytometry was used to measure the extent of C6 cellular uptake in A549 cells (Fig. 21A). The uptake amount of C6 in cells treated with C6-ALB-NPs ($p < 0.05$) and CTX-C6-ALB-NPs ($p < 0.001$) was significantly enhanced compared to C6 control-treated cells (Fig. 21B).

Moreover, the CTX-C6-ALB-NPs treated cells exhibited a significantly higher ($p < 0.001$) amount of C6 uptake as compared to C6-ALB-NPs. Overall, the findings of this study provide important insights into the cellular absorption mechanism of CTX-conjugated ALB-NPs. The increased uptake of C6 in cells treated with CTX-C6-ALB-NPs revealed active targeted delivery in A549 cells via EGFR-mediated endocytosis. These findings suggest that CTX-C6-ALB-NPs may be a promising approach for targeted OLA delivery in cancer therapy.

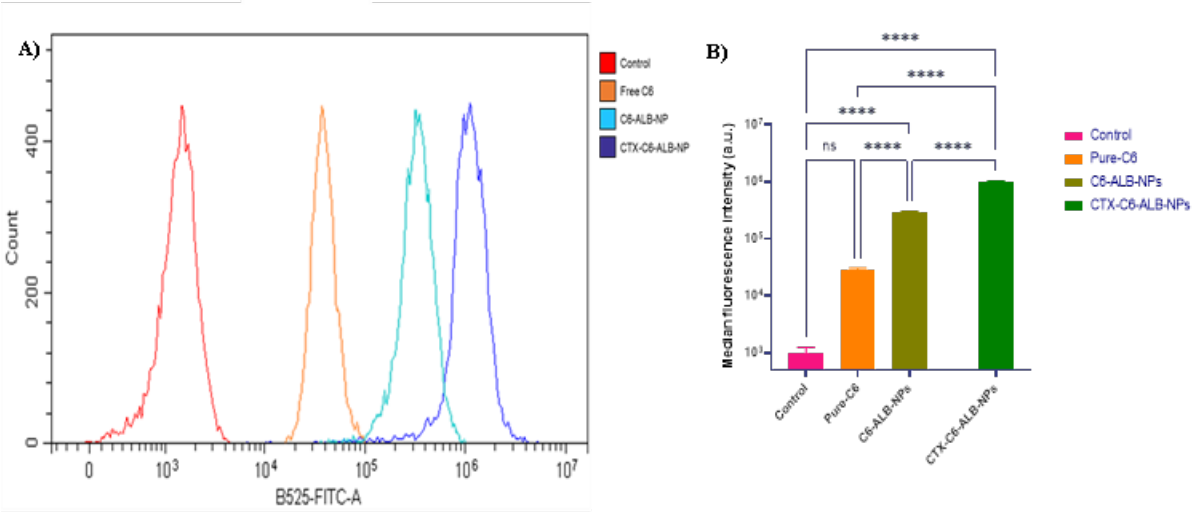

Figure 21 A) Flow cytometric analysis of A549 cells when incubated with control, Pure-C6, C6-ALB-NPs, CTX-C6-ALB-NPs incubated for 6 h. B) Fluorescence intensity of control, Pure-C6, C6-ALB-NPs, CTX-C6-ALB-NPs by flow cytometry. The results are expressed as means ± SD (n = 3).

3.11.6 Apoptosis analysis

Apoptosis represents as a programmed mechanism for the body to remove unwanted or abnormal cells, while necrosis can occur as an alternative to apoptosis under toxic conditions. Following a cytotoxicity assessment, we utilized fluorescence microscopy and staining methods involving Acridine orange (AO) and ethidium bromide (EtBr) to examine cell death modes by observing changes in the nucleus morphology of A549 cells (Fig. 22). To ascertain if cell death followed the apoptotic pathway, A549 cells were treated with pure OLA, OLA-ALB-NPs, and CTX-OLA-ALB-NPs at concentrations of 4.35 µg/mL for 24 hours.

Fluorescence microscopy revealed apoptotic characteristics such as nucleus shrinkage and chromatin condensation in A549 lung cancer cells treated with nanoparticles. Our investigation demonstrated that live cells exhibited an intact cell membrane, uniform chromatin, and nuclei emitting green fluorescence. Early apoptotic cells displayed fragmented nuclei and membrane blebbing, while cells in late apoptosis presented condensed chromatin, with nuclei showing an orangish or pale-yellow fluorescence. These findings also confirmed that A549 cells exhibited higher sensitivity to CTX-OLA-ALB-NPs compared to OLA-ALB-NPs or OLA alone. In contrast to cells treated with OLA and OLA-ALB-NPs, the majority of cells exposed to CTX-OLA-ALB-NPs were in either the early or late stages of apoptosis. These results supported the findings from the cytotoxicity study, indicating that cells were more responsive to CTX-OLA-ALB-NPs. The nanoparticles induced greater apoptosis in cells due to their specific targeting of lung cancer cells. Therefore, the analysis using AO/EtBr double staining strongly suggests that apoptosis was the primary mode of cell death induced by ALB-NPs in A549 cells.

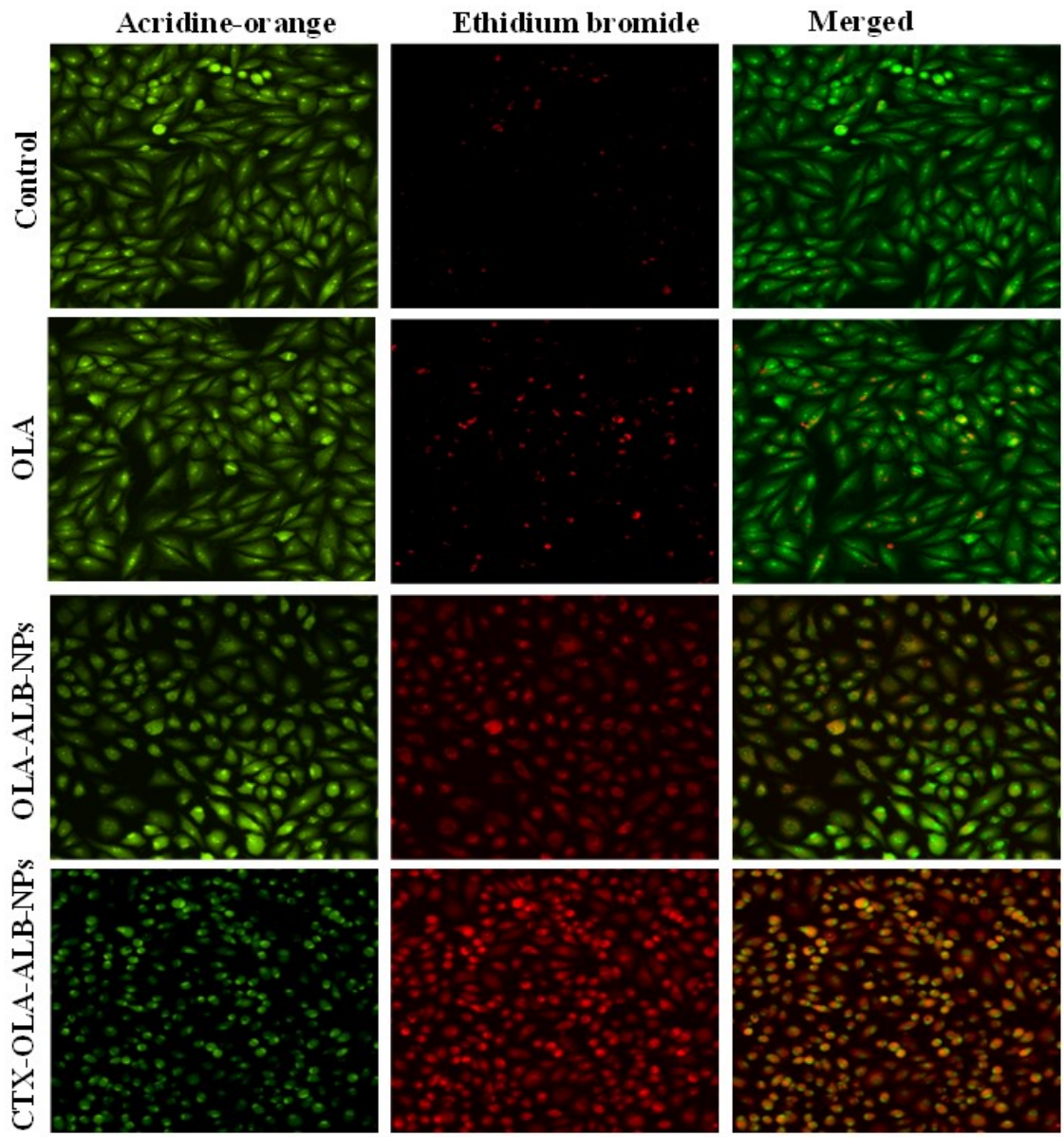

Figure 22 Cells morphological changes after treatment of free OLA, OLA-ALB-NPs and CTX-OLA-ALB-NPs in A549 cells

3.11.7 ROS generation assay

Reactive oxygen species (ROS) are potent oxidants known to initiate cell death by elevating intracellular reactive radicals, leading to oxidative degradation of DNA, proteins, and lipids. We assessed ROS levels using the green fluorescent probe DCFH-DA, revealing that untreated A549 cells did not generate intracellular ROS, unlike cells treated with OLA-ALB-NPs and CTX-OLA-ALB-NPs (Fig. 23). Interestingly, OLA exposure had no impact on ROS levels,

likely due to its heightened hydrophobicity, preventing its release into cells. OLA-ALB-NPs exposure led to a slight ROS increase in A549 cells, possibly due to the absence of a targeting agent like CTX. Strikingly, CTX-OLA-ALB-NPs exhibited significantly elevated ROS levels compared to OLA and OLA-ALB-NPs treatments, potentially causing cellular damage and ultimately triggering apoptotic cell death.

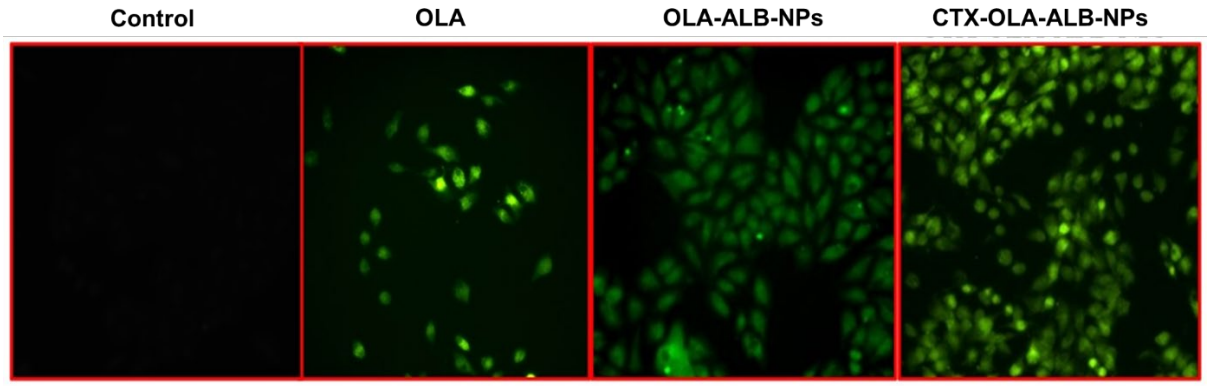

Figure 23 Detection of intracellular ROS by measuring fluorescent intensity in A549 cells using DCFH-DA probe (10 μg/mL) under fluorescence microscope.

3.11.8 Annexin V-Alexa fluor/Propidium iodide staining assay

Apoptosis is an intrinsic cellular process essential for normal development and maintaining an organism's equilibrium, making it a potential target for cancer therapy. To assess the extent of apoptosis induced by CTX-OLA-ALB-NPs in A549 cells, we employed an Annexin-V Alexa Fluor 488/Propidium iodide (PI) assay (170). When cells undergo apoptosis, phosphatidyl serine, an apoptosis marker, is exposed on the cell surface due to altered cell membrane permeability, and this exposure is detected using the Annexin reagent (177). The Annexin-V/Propidium iodide dual labeling method allows for the differentiation between apoptotic, living, and necrotic cells, while propidium iodide staining aids in distinguishing between late apoptotic and necrotic cells. The efficacy of OLA, OLA-ALB-NPs, and CTX-OLA-ALB-NPs to result in apoptosis in A549 cells was investigated at the IC_{50} value and incubation time based on the results from the MTT test. Fig. 24A shows the results of flow cytometric analysis after

24 h of treatment with OLA, OLA-ALB-NPs, and CTX-OLA-ALB-NPs. The figure (Fig. 24B) displays the percentage of cells population in different apoptotic phases such as early apoptotic population of cells was 14.8 ± 1.8%, 30.0 ± 2.0%, and 50.5 ± 2.2% and total apoptotic population of cells was 22.88 ± 0.9%, 45.33 ± 1.4%, 75.72 ± 2.1% in OLA, OLA-ALB-NPs, and CTX-OLA-ALB-NPs treated cells, respectively. In contrast, the necrotic populations were 2.7 ±1.5%, 3.8 ± 1.9%, and 0.22 ± 2.1% in OLA, OLA-ALB-NPs, and CTX-OLA-ALB-NPs treated cells, respectively. It indicates that CTX-OLA-ALB-NPs have superior cytotoxicity and a higher apoptotic potential than OLA and OLA-ALB-NPs on human lung cancer cells (A549).

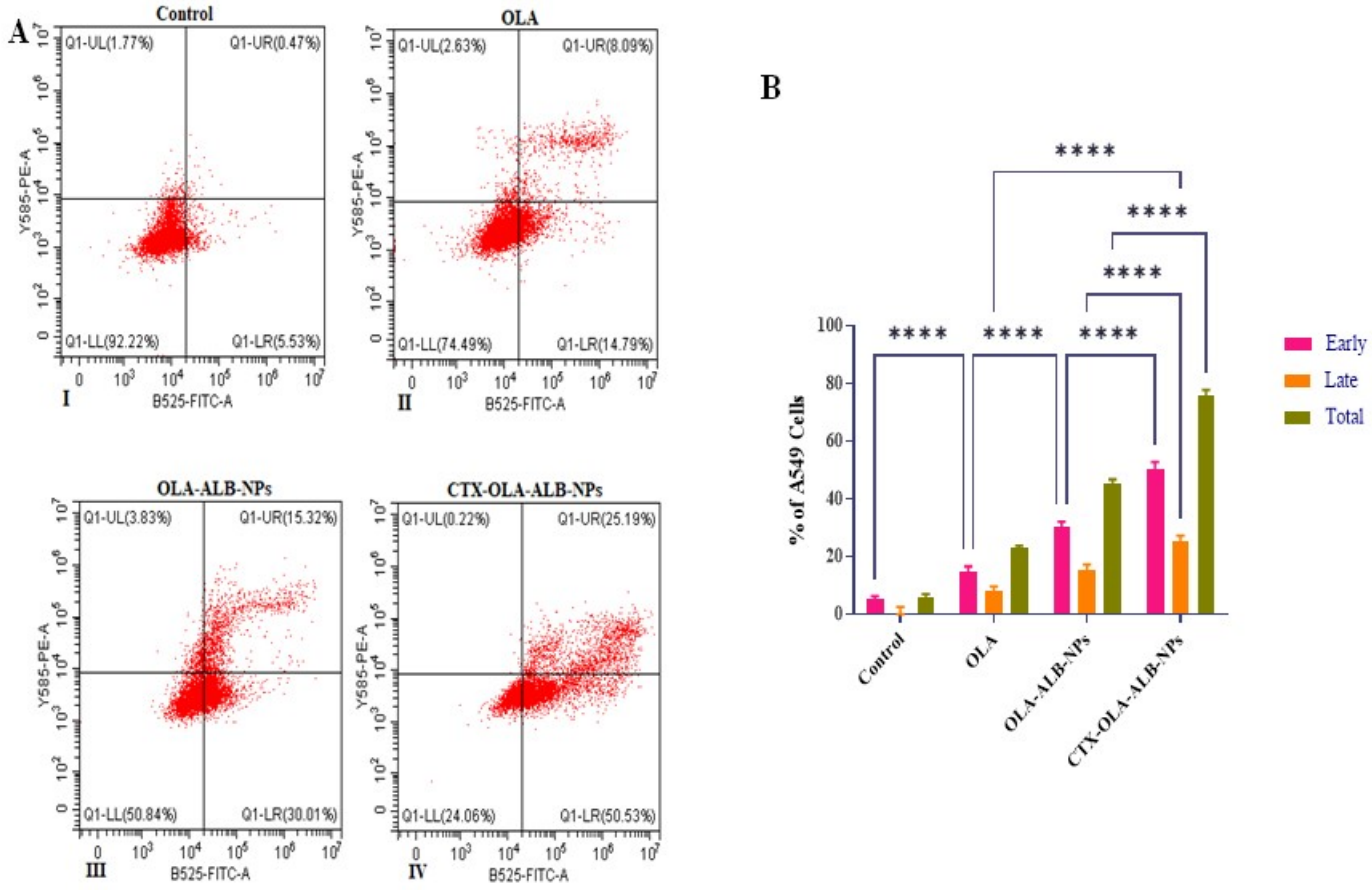

Figure 24 A) Flow cytometric analysis of control and treated A549 cells with same concentrations of OLA, OLA-ALB-NPs, and CTX-OLA-ALB-NPs. Dual staining with AnnexinV/PI distinguishes the percentage of cells at various phases. B) Statistical analysis has been performed by using one-way ANOVA followed by Tukey test. Here *, **, ***, and **** represents significant difference at $p < 0.05$, 0.01, 0.001 and 0.0001, respectively, as compared to control.

3.11.9 Cell cycle analysis

The effect of OLA-ALB-NPs and CTX-OLA-ALB-NPs on the different phases of cell cycle of A549 cells was studied using flow cytometry and the propidium iodide staining method (178). By analysing A549 cells percentages at different phases, we determined that OLA-ALB-NPs, and CTX-OLA-ALB-NPs primarily caused blockage at the G1 phase of the cell cycle of A549 cells as the G0/G1 ratio increasing to 69.5 ± 2.1%, and 79.6 ± 1.8% in OLA-ALB-NPs, and CTX-OLA-ALB-NPs treated cells respectively (n = 3), compared to the control cells (58.6 ± 2.4%). Thus, both the percentage of cells in S-phase as well as the G2/M ratio were lower than in control cells (Fig. 25).

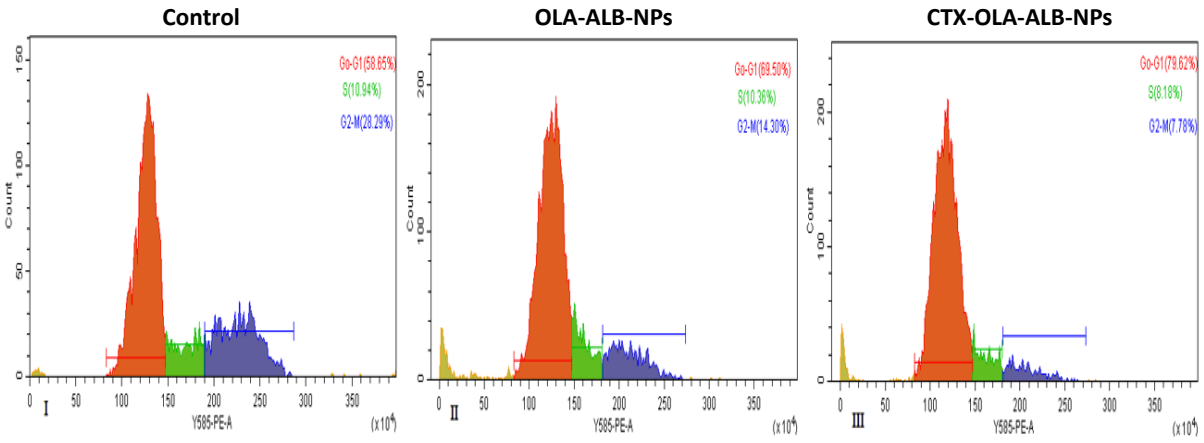

Figure 25 depicts the population of A549 cells at various stages of the cell cycle after 24 h treatment with OLA-ALB-NPs and CTX-OLA-ALB-NPs.

3.12 *In vivo* studies

3.12.1 Pharmacokinetic study

An *in vivo* pharmacokinetic study was conducted on Wistar rats to assess OLA control, OLA-ALB-NPs, and EGFR-targeted CTX-OLA-ALB-NPs. Rats were intravenously administered NPs containing 10 mg/kg equivalents of OLA at different time intervals, and the plasma OLA concentration versus time curve was plotted (Fig. 26). The findings revealed that both ALB-

NPs had approximately 2 times higher relative bioavailability compared to the OLA control (Table 8). The pharmacokinetic profile of CTX-OLA-ALB-NPs exhibited a prolonged half-life ($T_{1/2}$) and mean residence time in comparison to OLA ($p < 0.05$). Additionally, ALB-NPs, apart from the OLA control, demonstrated significantly lower clearance rates and volumes of distribution (V_d). This reduced V_d value could be attributed to the controlled release of OLA from the ALB-NPs matrix, contrasting with the aqueous OLA suspension in the OLA control, which resulted in higher V_d values (179, 180).

Table 8 Pharmacokinetic parameters of OLA and OLA-ALB-NPs, CTX-OLA-ALB-NPs

Parameters	**OLA (Mean ± SD*)**	**OLA-ALB-NPs (Mean ± SD*)**	**CTX-OLA-ALB-NPs (Mean ± SD*)**
AUC $_{total}$ (ng.h/ml)	31195.85 ± 1127.16	68557.01± 1424.36	73592.78± 1148.57
C $_{max}$ (ng/ml)	10547.72 ± 2041.71	9046.88± 1772.63	9354.99± 1780.43
$T_{1/2}$ (h)	8.40± 0.54	9.67± 2.78	10.27± 2.34
MRT (h)	5.412± 0.38	15.717± 3.58	16.706± 3.80
V_d (l/kg)	0.917 ± 0.02	0.383± 0.03	0.401 ± 0.02
Cl $_{total}$ (ml/kg.h)	75.65 ± 1.13	27.436 ± 0.74	25.045± 0.67
K_E (h^{-1})	0.083 ± 0.003	0.072 ± 0.001	0.067 ± 0.002
F_R	-	2.18	2.36

OLA: Oleanolic acid, OLA-ALB-NPs: Oleanolic acid loaded albumin nanoparticles, CTX-OLA-ALB-NPs: CTX conjugated Oleanolic acid loaded albumin nanoparticles, MRT: Mean residence time, V_d: Volume of distribution, Cl total: Total body clearance, C_{max}: maximum plasma concentration, T_{max}: time to reach C_{max}; AUC total: area under plasma drug concentration-time curve; $T_{1/2}$: biological half-life; K_E: Elimination rate constant (fraction of drug in an animal that is eliminated per unit of time); F_R: Relative bioavailability. *n = 3.

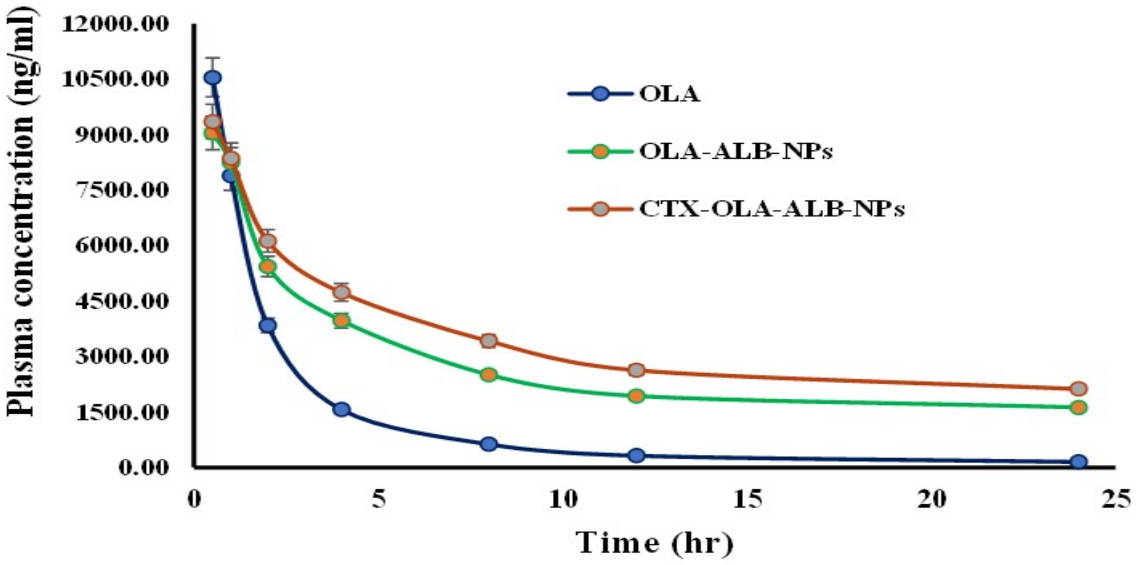

Figure 26 Pharmacokinetic analysis of OLA control, non-targeted, and EGFR targeted NP after *i.v.* administration (10 mg/kg *i.v.*, n = 3) in Wistar rats

3.12.2 Histopathology

Numerous histopathological investigations have provided evidence of the toxicity associated with conventional clinical formulations of anticancer medications like docetaxel, paclitaxel, and doxorubicin when administered to animals. In our study, the control group of Wistar rats, which received a normal saline solution, did not display any pathological abnormalities in essential organs such as the heart, lungs, liver, and kidneys. Conversely, the groups of Wistar rats that received multiple intravenous injections of OLA control, non-targeted ALB-NPs, and targeted ALB-NPs over a 14-day period exhibited only mild lesions in vital organs, indicating a safer profile (Fig. 27). These findings suggest that TPGS may have enhanced the compatibility of CTX-OLA-ALB-NPs with lung tissue, potentially reducing their toxicity.

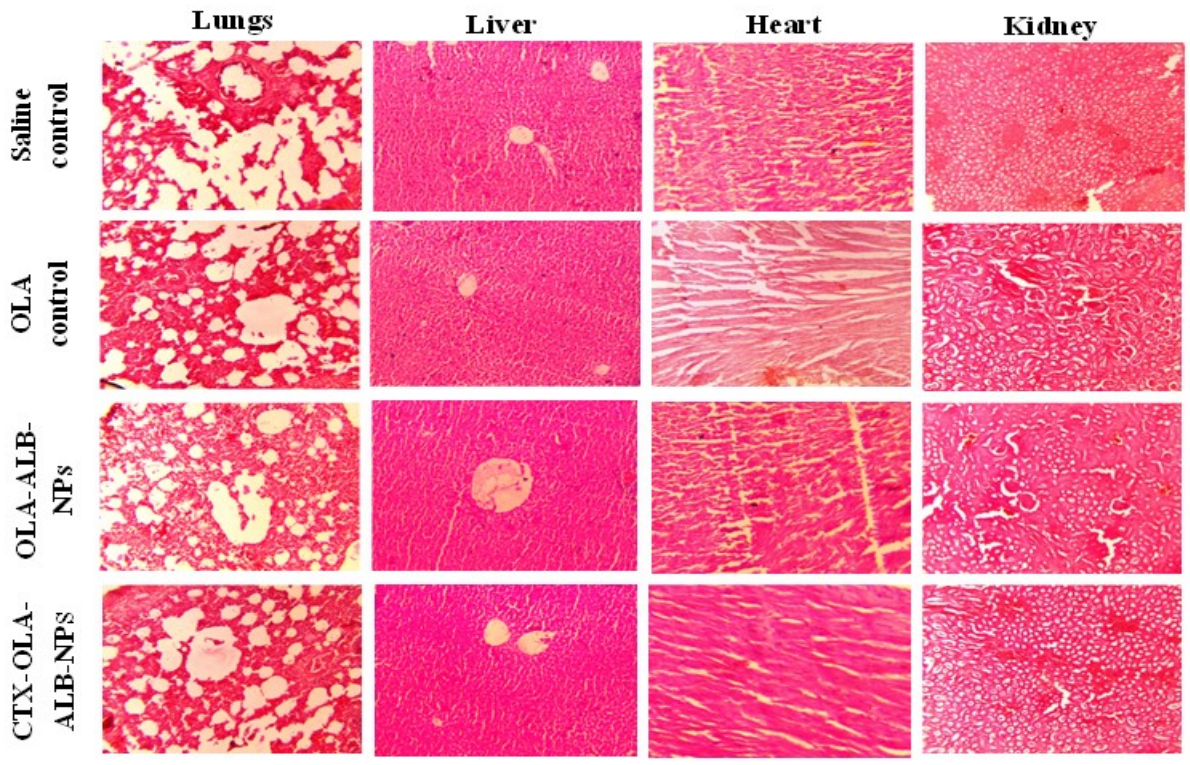

Figure 27 H&E-stained microscopic images of vital organs of animals treated with Saline control, OLA control, non-targeted OLA-ALB-NPs and targeted CTX-OLA-ALB-NPs.

3.12.3 *In vivo* safety using bronchoalveolar lavage (BAL) fluids of rats

Alkaline phosphatase (ALP) activity is a well-known measure used to evaluate the secretion activity of type II alveolar epithelial cells. Increased ALP levels in bronchoalveolar lavage (BAL) fluids have been associated with toxicity in these cells. Consequently, monitoring ALP activity in BAL fluids serves as a valuable indicator of potential damage to type II cells. Lactate dehydrogenase (LDH), an enzyme primarily located in cell cytoplasm, is widely employed as a biomarker to assess cellular injury due to its presence in various tissues and its rapid release into the bloodstream following cellular damage. LDH stands as a dependable marker for tissue damage and has been extensively studied in diverse pathological conditions. Its measurement has proven useful in diagnosing, prognosing, and monitoring several diseases, including myocardial infarction, liver diseases, and cancer. Therefore, LDH is an invaluable tool in both

clinical practice and research for evaluating cellular injury and disease progression. To assess the safety of OLA, OLA-ALB-NPs, and CTX-OLA-ALB-NPs as potential treatments for lung cancer, a thorough examination of lung toxicity parameters was conducted, as illustrated in Fig. 28. In this investigation, lung toxicity indicators of OLA-ALB-NPs were monitored at intervals of 0, 7, and 15 days post-intravenous administrations. The findings revealed that both OLA-ALB-NPs and CTX-OLA-ALB-NPs did not induce significant lung toxicity in comparison to the OLA-treated group. This was evident from the levels of various pulmonary toxicity markers, such as ALP and LDH, in the bronchoalveolar lavage fluid of rats. After 7 days, a significant increase in ALP ($p \leq 0.05$) and LDH ($p \leq 0.01$) levels was observed in the OLA group compared to the control group. This increase could be attributed to OLA's limited solubility in aqueous environments, leading to the generation of reactive oxygen species (ROS) in lung cells.

However, after 15 days, no significant difference was observed in ALP and LDH levels in the treatment group of OLA compared to animal groups treated with saline. Although, there was no significant difference between the levels of ALP and LDH in BAL fluids of animals treated with OLA, OLA-ALB-NPs, and CTX-OLA-ALB-NPs, as compared to animals treated with saline. These findings suggest that OLA-ALB-NPs and CTX-OLA-ALB-NPs did not increase the ALP and LDH levels due to their controlled release mechanism of OLA, indicating their safety.

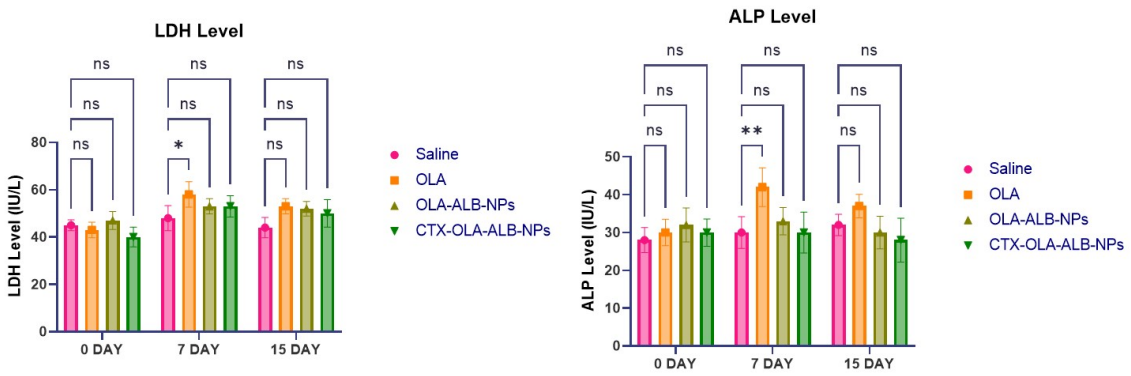

Figure 28 LDH and ALP levels in rats at day 0, day 7, and day 15 after administration of saline, OLA, OLA-ALB-NPs and CTX-OLA-ALB-NPs.

3.12.4 *In vivo* lung cancer targeting efficacy

The green photoacoustic signals indicated the presence of the NPs in the lung tissue (Fig. 29). B(a)P cancer animals treated with MB control, MB-ALB-NPs and CTX-MB-ALB-NPs had lung areas with photoacoustic signal intensities of 2.44 ± 0.12 %, 6.31 ± 0.15 % and 12.72 ± 0.27 %, respectively. In contrast, control mice (without MB) do not show any green fluorescent signal. The fraction of photoacoustic signals that can be used to infer where MB and MB-loaded NPs are distributed in the body. Thus, the outcomes of the findings revealed that the CTX-MB-ALB-NPs show higher photoacoustic signals ($p < 0.001$) as compared to MB control and MB-ALB-NPs.

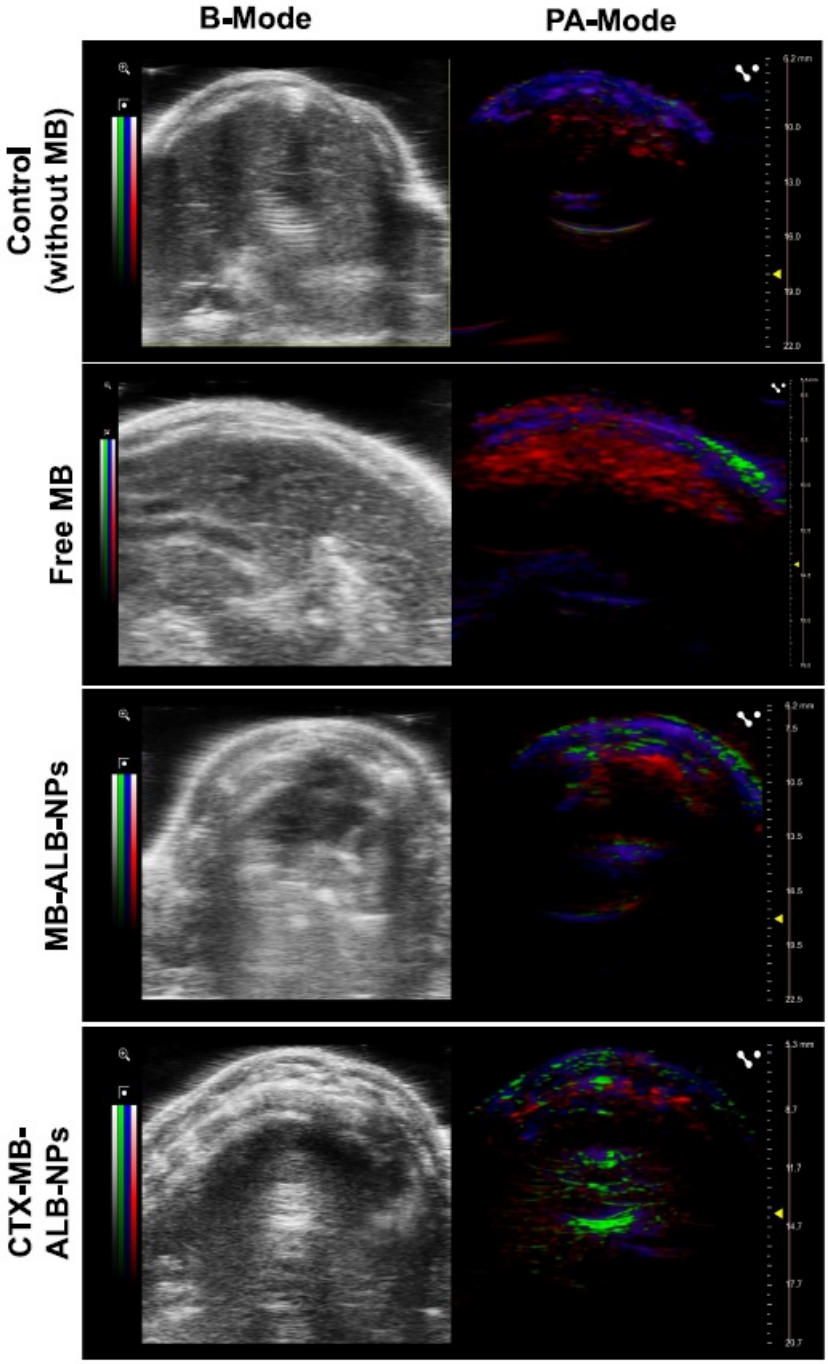

Figure 29 . Ultrasound (B-mode, left panel) and photoacoustic (PA mode, right panel) imaging of B(a)P induced lung cancer in mice after 30 min of administration of free MB and MB loaded NPs. Red, blue and green signal in the left panel indicates oxy-hemoglobin, deoxy-hemoglobin and MB, respectively